Geology and wall rock alteration at the Hercynian Draa Sfar Zn–Pb–Cu massive sulphide deposit, Morocco

Abdelhay Belkabir, Harold L. Gibson, Eric Marcoux, David Lentz, S. Rziki

Geology and wall rock alteration at the Hercynian Draa Sfar Zn–Pb–Cu massive sulphide deposit, Morocco

A. Belkabir[a], H.L. Gibson[b], E. Marcoux[c], D. Lentz[d] and S. Rziki[e]
[a]Faculté des Sciences et Techniques de Marrakech, Département des Sciences de la Terre, B.P. 549, Av. Abdelk. Khattabi, Marrakech, 40000 Morocco
[b]Mineral Exploration Research Centre, Department of Earth Sciences, Laurentian University, Sudbury, Ontario, Canada P3E 2C6
[c]ISTO Géosciences, Université d'Orléans, B.P. 6759, 45067 Orléans cedex 2, France
[d]Dept. of Geology, University of New Brunswick, Box 4400, 2 Bailey Drive, Fredericton, New Brunswick, Canada E3B 5A3
[e]Mine Draa Sfar, Marrakech, Morocco

Abstract

Draa Sfar is a siliciclastic–felsic, volcanogenic massive sulphide (VMS) Zn–Pb–Cu deposit located 15 km north of Marrakesh within the Jebilet massif of the western Moroccan Meseta. The Draa Sfar deposit occurs within the Sarhlef series, a volcano-sedimentary succession that hosts other massive sulphide deposits (*e.g.*, Hajar, Kettara) within the dominantly siliciclastic sedimentary succession of the lower Central Jebilet. At Draa Sfar, the footwall lithofacies are dominated by grey to black argillite, carbonaceous argillite and intercalated siltstone with localized rhyodacitic flows and domes, associated *in situ* and transported autoclastic deposits, and lesser dykes of aphanitic basalt and gabbro. Thin- to thick-bedded, black carbonaceous argillite, minor intercalated siltstone, and a large gabbro sill dominate the hanging wall lithofacies. The main lithologies strike NNE–SSW, parallel to a pronounced S1 foliation, and have a low-grade, chlorite–muscovite–quartz–albite–oligoclase metamorphic assemblage. The Draa Sfar deposit consists of two stratabound sulphide orebodies, Tazakourt to the south and Sidi M'Barek to the north. Both orebodies are hosted by argillite in the upper part of the lower volcano-sedimentary unit. The Tazakourt and Sidi M'Barek orebodies are highly deformed, sheet-like bodies of massive pyrrhotite (up to 95% pyrrhotite) with lesser sphalerite, galena, chalcopyrite, and pyrite. The Draa Sfar deposit formed within a restricted, sediment-starved, fault-controlled, anoxic, volcano-sedimentary rift basin. The deposit formed at and below the seafloor within anoxic, pelagic muds.

The argillaceous sedimentary rocks that surround the Draa Sfar orebodies are characterized by a pronounced zonation of alteration assemblages and geochemical patterns. In the more proximal volcanic area to the south, the abundance of medium to dark green chlorite progressively increases within the argillite toward the base of the Tazakourt orebody. Chlorite alteration is manifested by the replacement of feldspar and a decrease in muscovite abundance related to a net addition of Fe and Mg and a loss of K and Na. In the volcanically distal and northern Sidi M'Barek orebody alteration within the footwall argillite is characterized by a modal increase of sericite relative to chlorite. A calcite–quartz–muscovite assemblage and a pronounced decrease in chlorite characterize argillite within the immediate hanging wall to the entire Draa Sfar deposit. The sympathetic lateral change from predominantly sericite to chlorite alteration within the footwall argillite with increasing volcanic proximity suggests that the higher temperature part of the hydrothermal system is coincident with a volcanic vent defined by localized rhyodacitic flow/domes within the footwall succession.

Keywords: Massive sulphide; Draa Sfar; Hercynian; Hydrothermal alteration; Morocco

1. Introduction

The newly opened (2005) Draa Sfar massive sulphide deposit, located in the southeastern margin of the Hercynian Jebilet massif, is one of two principal Zn producers in Morocco (Fig. 1). The Draa Sfar deposit is a sheet-like, massive sulphide deposit hosted within the Sarhlef series, a terrigeneous, sediment-dominated, volcano-sedimentary succession consisting of carbonaceous argillite, argillite, siltstone and sandstone with subordinate volcanic and volcaniclastic rocks (Huvelin, 1977). The massive sulphide deposit occurs near the top of an argillite–siltstone succession that conformably overlies a rhyodacite dome complex and associated volcaniclastic rocks and is conformably overlain by carbonaceous argillite. The Draa Sfar deposit is overturned, dips steeply to the east and faces west (Fig. 2). The massive sulphide deposit consists of two, highly deformed, sheet-like orebodies, Tazakourt and Sidi M'Barek, that combined have a total strike length of 1.5 km. Only Tazakourt has been developed and is currently in production. It has an average thickness of 20 m and an N–S strike length of 1 km (Fig. 2). Boudinage of the Tazakourt massive sulphide lens has resulted in several, *en echelon*, moderately north-plunging lenses.

In this paper we present the results from mapping, petrographic, mineralogical (X-ray diffraction), electron microprobe (EPMA) and geochemical studies of the sedimentary and volcanic lithofacies and alteration assemblages that host the Draa Sfar deposit. Our objectives are: (1) to provide the first reconstruction of the volcano-sedimentary environment in which the Draa Sfar deposit formed; (2) to describe the mineralogy, composition and distribution of hydrothermal alteration assemblages, particularly those that developed within the sedimentary lithofacies as they are only sparsely documented in the literature; and (3) to compare the pyrrhotite-rich Draa Sfar deposit to the more common and larger pyritic massive sulphide deposits of the Iberian Pyrite Belt, which share a similar age, sedimentary host rocks, and tectonic setting. This paper is complemented by a second contribution that focuses on the mineralogy, composition and origin of the sulphide ores at Draa Sfar (Marcoux et al., 200X).

2. Geological setting

The Draa Sfar mine is located along the southern margin of the Jebilet massif, in the southern part of the west Moroccan Meseta (Fig. 1a). The Jebilet massif, which extends for 170 km E–W and 40 km N–S, has been interpreted as a Devono-Carboniferous, intra-continental, rift basin (Huvelin, 1977, Beauchamp, 1984, Aarab and Beauchamp, 1987, Piqué and Michard, 1989 and Beauchamp et al., 1991). The Jebilet massif consists of three lithotectonic domains, the western, central, and eastern domains (Fig. 1b) that are separated by major shear zones (Huvelin, 1977 and Lagarde and Choukroune, 1982). The western domain consists of Cambrian and Ordovician rocks, whereas the central domain consists of metamorphosed and deformed upper Visean rocks. The eastern domain is also composed of Visean rocks, but is covered by a series of nappes that contain strata ranging from Ordovician to Early Carboniferous in age.

The Central Jebilet domain contains a thick succession of argillite and carbonaceous argillite (up to 1.5 km thick), representing the lower part of the succession, overlain by Carboniferous carbonaceous argillites and limestones (< 100 m) that define the top of an interpreted basin-fill succession (Bordonaro, 1983). Beauchamp et al. (1991) interpreted the argillites of Central Jebilet to have been deposited in an anoxic, “shallower” water environment. The end of the Carboniferous was also characterized by three types of magmatic activity (Bordonaro, 1983, Aarab and Beauchamp, 1987 and Bernard et al., 1988): (1) bimodal, subvolcanic, rift-related

tholeiitic gabbro and minor rhyodacite and rhyodacite flows; (2) syntectonic calc–alkaline granite intrusions and (3) post-tectonic dykes and sills of microdiorite (Huvelin, 1977, Bernard et al., 1988 and Essaifi et al., 2004).

Deformation in the Central Jebilet is marked by a Hercynian, D_1, E–W shortening that is responsible for the orientation of the N-striking, transposed strata, development of the main regional S_1 schistosity (striking N–S and subvertical), regional folds that trend 030°, and the emplacement of syntectonic granites. The D_1 deformation was associated with low-grade regional metamorphism, typified by a quartz–muscovite–chlorite assemblage. D_1 shortening was followed by an N–S D_2 shortening (S_2 crenulation cleavage) and late brittle deformation (Huvelin, 1977, Bordonaro, 1983, Bernard et al., 1988 and Essaifi et al., 2004).

Several massive sulphide deposits, including Draa Sfar, are hosted by the volcano-sedimentary succession within the central domain (Fig. 1b). The deposits are stratiform, characterized by a sulphide mineralogy dominated by pyrrhotite (90 to 95% of total sulphides), and range from Zn-rich polymetallic mineralization (*e.g.*, Koudiat Aicha deposit — 4.5 Mt at 2.7% Zn, 1.2% Pb and 0.6% Cu; Draa Sfar mine — 10 Mt at 5% Zn, 1.2% Pb and 0.5% Cu), to low-grade sulphide deposits (*e.g.*, Kettara; 30 Mt of pyrrhotite at 0.7% Cu). The sulphide deposits are pre-tectonic, they are affected by S_1 schistosity and generally occur as folded and dislocated sheet-like orebodies (Bordonaro, 1983 and Bernard et al., 1988).

Massive sulphide deposits of the Jebilet and Guemassa massifs (Fig. 1a, b) have been compared to those of the Iberian Pyrite Belt (IPB) (Bordonaro et al., 1979, Bernard et al., 1988 and Lescuyer et al., 1998; see also Fig. 2 in the latter publication). Similarities between the massive sulphide districts include: (1) age, in spite of the apparent diachronous ages of the IPB (late Devonian to Visean) and Moroccan deposits (*Dinantian*), it is possible to define a main metallogenic "peak" around 350 Ma that followed the major phase of Devonian compression; (2) both occur in largely siliciclastic-dominated successions with a higher proportion of felsic to mafic volcanic rocks in the IPB, where that latter typically occur as sills; and (3) geodynamic setting, as both the Iberian and Morroccan massive sulphide deposits are interpreted to have formed in an epicontinental rift within the outer zone of the Hercynian belt (Lescuyer et al., 1998).

3. Geology of the Draa Sfar deposit

The Central Jebilet succession has been subdivided into a lower volcano-sedimentary succession, the Sarhlef series and an upper sedimentary succession, the Teksim series (Huvelin, 1977 and Bordonaro, 1983). The Draa Sfar deposit is located in the upper part of the Sarhlef series (Fig. 2 and Fig. 3) and is underlain by more than 500 m of strata consisting of carbonaceous argillite, argillite, intercalated siltstone and a subordinate, but locally dominant coherent rhyodacite and associated volcaniclastic facies. The footwall succession also contains thin, aphanitic mafic dykes. The Draa Sfar deposit is conformably overlain by a thinly bedded carbonaceous argillite and intercalated siltstone lithofacies that is locally intruded by a large gabbro sill (Fig. 2). The lithologies strike NNE–SSW and have a layer-parallel S_1 foliation (Fig. 4). Within the least-deformed volcanic and sedimentary rocks, younging directions are easily identified from primary structures (cross bedding, grading, and synsedimentary loading structures) that consistently indicate that the strata immediately above and below the deposit are overturned and young to the west (Fig. 2). However, on a larger scale, mapping, lithofacies correlation (*e.g.*, coherent rhyodacite to volcaniclastic facies) and facing directions indicate that the strata are folded about a north-trending F_1 anticline that

places the Draa Sfar deposit on the west limb of this fold (Fig. 2 and Fig. 3). The lithologies contain mineral assemblages dominated by chlorite, muscovite, quartz, albite and rare oligoclase–orthoclase indicative of a low metamorphic grade. The volcano-sedimentary rocks of the Draa Sfar deposit typically lack internal stratigraphic marker units, but display high lateral continuity.

3.1. Footwall volcanic lithofacies

Coherent rhyodacite and volcaniclastic rocks are the dominant volcanic lithofacies within the footwall. The coherent rhyodacite lithofacies has a strike length of approximately 600 m, a maximum thickness of 400 m (Fig. 2), and consists of weakly foliated, massive to locally flow-banded (with amygdule-rich bands) rhyodacite (Fig. 5a). The rhyodacite displays local *in situ* brecciation (Fig. 5b). Abundant spherulites indicate that the rhyodacite was glassy prior to devitrification. Quartz phenocrysts (2–3%) are typically subhedral, whereas albite occurs as euhedral phenocrysts (Ab_{99}–Ab_{91}) and as felted laths in the microgranular, spherulitic groundmass. The base of the coherent rhyodacite is a monomictic, *in situ* brecciated to angular clast-rotated breccia that is interpreted to be an autobreccia that developed along the base of the coherent rhyodacite flow/dome. The coherent rhyodacite flow/dome and autobreccia facies dominates the east limb of the north-plunging anticline where it occurs in the footwall below the southern part of the Tazakourt orebody. Crudely layered and poorly size-sorted rhyodacitic volcaniclastic rocks dominate the west limb and nose of the anticline. The volcaniclastic rocks consist of framework-supported units of lapilli tuff, lapillistone, and angular, block-rich (blocks up to 50 cm), tuff breccia, using the non-genetic, granulometric classification and nomenclature of Fisher (1966). The clasts are all rhyodacitic, but individual depositional units (< 1 to 5 m thick) are distinguished by variations in the type (quartz and or feldspar) and abundance of phenocrysts within clasts and crystals within the breccia matrix. Volcaniclastic units that contain clasts with a phenocryst type and content similar to that of the coherent rhyodacite are interpreted as flank breccias to the coherent rhyodacite derived through mass wasting of the dome, with their emplacement as gravity-driven, high concentration mass flows. Identical units with different phenocryst populations are interpreted to have a similar origin but different provenance, perhaps from unexposed phases of the coherent rhyodacite, or from yet unidentified flows or domes. Thin (from < 1 mm up to 1–2 cm), crystal tuff and locally crystal-lithic tuff (< 10% felsic lapilli) units are intercalated with the argillite siltstone lithofacies that immediately underlies the Draa Sfar deposit (and that presumably covers the coherent and volcaniclastic lithofacies) along its entire strike length. The crystal-lithic tuffs and crystal tuffs contain crystals of quartz and albite (up to 1 mm in size) and minor K-feldspar (the latter indicated by X-ray diffractometry) in the matrix and within vitroclastic to perlitic rhyodacitic lapilli that now consist of chlorite, quartz, calcite, muscovite, and minor biotite. The tuff and crystal tuff units were emplaced as low concentration mass flows-turbidites based on their normal grading and incorporation of argillaceous sediment that locally give the units a darker grey to black colour. They may represent distal deposits derived through mass wasting of rhyodacitic flows or domes, or perhaps they are pyroclastic in origin, in the latter case they may represent primary pyroclastic deposits or redeposited syneruptive deposits.

3.2. Footwall argillite–siltstone lithofacies

The footwall argillite–siltstone lithofacies consists of black carbonaceous argillite, green to light grey argillite with intercalated siltstone, and rare sandstone beds that are moderately to highly schistose (now phyllites and fine-grained schists with S_1 and S_2 well developed; Fig.

6a, b). The mineralogy is dominated by a quartz–chlorite–muscovite–albite assemblage in microcrystalline layers. The proportion of chlorite and muscovite is variable resulting in chlorite-dominated or muscovite-dominated beds (Fig. 6d, f). Disseminated sulphides and flattened, cm-sized sulphide nodules are common in the argillite and siltstone (Fig. 6f). Siltstone and rare sandstone occur as thinly bedded to laminated layers that are often boudinaged and range from 10 to 60 cm in thickness. These layers are composed of quartz grains (up to 80%), chlorite, muscovite, and smaller grains of epidote, calcite, opaques, titanite, leucoxene, and zircon (Fig. 6a, b, e). The siltstone beds are locally interstratified with siltstone laminae containing disseminated sulphides or with laminae of massive sulphide (Fig. 6c). The siltstone and sandstone beds are more common in the southern part of the mine, closer to the underlying coherent rhyodacite and volcaniclastic lithofacies. Beauchamp et al. (1991) interpreted the coherent rhyodacitic to have acted as a topographic "barrier" separating sediments derived from the south and depositing detritus near the flow-dome from pelagic sediments to the north.

At Draa Sfar North, a subunit of gray-coloured, bioclastic argillite (10 to 15 m thick) is recognized within the argillite–siltstone lithofacies in drill core (*e.g.*, DS-132, DS-131; Fig. 2). This subunit is distinguished from other argillites by calcite enrichment in the form of disseminated, mm-sized "nodules" and brachiopod clasts recrystallized to quartz and calcite within a quartz–chlorite–muscovite–leucoxene-dominated matrix.

3.3. Hanging-wall carbonaceous argillite–minor siltstone lithofacies

The massive sulphide deposit is overlain by a 20 to 80 m thick, argillite–siltstone unit that is similar to the footwall argillite–siltstone lithofacies. This, in turn, is conformably overlain by a black to dark grey, carbonaceous argillite–minor siltstone lithofacies that displays rhythmic laminations of calcite as beds 2 mm to 1 cm in thickness (20 to 60% of the rock), which are transposed parallel to S_1 (Fig. 6g). The carbonaceous argillite consists of a fine-grained assemblage of muscovite, calcite, quartz and minor chlorite and leucoxene. This facies is a distinct marker that defines the top of the sulphide-bearing argillite–siltstone–volcaniclastic succession that is host to the Draa Sfar deposit (Fig. 3). The carbonaceous argillite regionally represents the lower part of the Teksim series, which has been interpreted as a rift basin-fill succession by Huvelin (1977).

3.4. Intrusions

Porphyritic, melagabbro (dolerite) dykes, from 0.3 to 1 m thick, with well preserved ophitic textures occur within the footwall argillite–siltstone lithofacies. The dykes are characterized by a metamorphic assemblage of actinolite–hornblende (50%), chlorite (15%), albite (15%), epidote (5%), and 5 to 10% titanite–leucoxene. Large actinolite grains form pseudomorphs after hornblende. Aphanitic basaltic dykes (0.4 to 0.8 m thick) are typically highly deformed, have a lepidoblastic texture, are composed of chlorite (70%) and rounded albite crystals (20 to 25%), and occur within the footwall rhyodacite–volcaniclastic and argillite–siltstone lithofacies. A large gabbro sill occurs in the carbonaceous argillite–minor siltstone lithofacies of the hanging wall succession (Fig. 2). It is moderately foliated along its margins and is fractured within its interior. The gabbro has a strike length of at least 600 m (N–S striking) and is displaced by late EW and NE faults. It is melanocratic, coarse-grained to porphyritic, and is characterized by blue interstitial quartz.

3.5. Structure

Structural evolution of the Draa Sfar deposit must be considered in the context of the complex tectonic history of the Hercynian Central Jebilet (Huvelin, 1977, Lagarde and Choukroune, 1982, Bordonaro, 1983, Bernard et al., 1988 and Essaifi et al., 2004). The textures of the volcanic and sedimentary lithofacies largely reflect their primary mineralogy. For example, grains of quartz and albite in the metasediments, and corroded quartz and albite phenocrysts in the metavolcanic units are ubiquitous and are interpreted to be primary. However, Draa Sfar has been affected by at least three phases of deformation. East–West D_1 compression represents the main phase of Hercynian deformation. It is responsible for tight isoclinal folding, transposition of strata, development of penetrative S_1 foliation (N10° to 75°), and m-scale, isoclinal F_1 folds that are sub-parallel to bedding (N10° to 15°), and dip steeply to the north (N50° to 60°). D_1 represents the principal phase of deformation in the mine area and has affected the main lithologies producing local boudinage of the massive sulphide orebodies and the prominent, north-plunging, F1 anticline in the mine area. D_1 is synchronous with low-grade, regional metamorphism responsible for the formation of muscovite and chlorite that define the S_1 foliation. North–South shortening attributed to D_2 is evident by an S_2 crenulation cleavage (N110° to 80°) and E–W-trending subvertical kink bands. S_2 is restricted to the more schistose rocks. A late brittle D_3 faulting event is manifested by conjugate sets of dextral and sinistral faults (EW and NNW). The late brittle deformation is also characterized by tensional vein sets and a rare S_3 cleavage that strikes ENE and dips steeply to the east.

3.6. Sulphide mineralization

The pyrrhotite-rich Draa Sfar deposit consists of two main, sheet-like, massive sulphide orebodies (Fig. 7). The south orebody, Tazakourt, is Zn-rich (8 to 9% Zn, 0.30% Cu and 1 to 2% Pb) and extends for more than 1 km in an N–S direction (Fig. 2). The north orebody, Sidi M'Barek, consists of two parallel pyrrhotite-rich massive sulphide lenses (Fig. 7). The western or upper lens is Zn-rich (6 to 7% Zn, ~ 0.3% Cu and < 1% Pb) and, based on stratigraphic correlation, is interpreted to represent the continuation of the Tazakourt orebody. The eastern or lower lens is Cu-rich (2 to 3% Cu, < 1% Zn, < 1% Pb and ~ 600 to 700 ppm Co). Total reserves at Tazakourt are estimated at 10 Mt grading 5.3% Zn, 2% Pb, and 0.5% Cu. Sidi M'Barek is yet to be delineated and the description that follows is based on underground mapping and mapping of drill core at Tazakourt, except where specified.

The sulphide orebodies occur along the western limb of a large, N-plunging, F_1 anticline (Bernard et al., 1988; this study). The orebodies are boudinaged and mylonitized and display a “pinch and swell” morphology along their strike length. The contacts of the orebodies are areas of high strain and often show pronounced shearing that is parallel to S_1 and post-S_1 chlorite–quartz veins. In addition, the massive sulphide often contains deformed inclusions consisting of dark chlorite and talc.

The sulphide orebodies are dominantly composed of pyrrhotite (70 to 95% sulphides), with lesser ferrous sphalerite (1 to 5%), galena (0.5 to 4%) and chalcopyrite (1 to 3%), except for the Cu-rich Sidi M'Barek orebody where the chalcopyrite content is locally 15%. Pyrite and marcasite are rare (< 1 vol.% of sulphides) at Tazakourt but are more common in the Cu-rich, lower Sidi M'Barek orebody (2 to 3 vol.%). Although rare framboidal pyrite may be primary, Marcoux et al. (200X) have interpreted the bulk of the pyrite as secondary, a product of the oxidative alteration of pyrrhotite. The thin (mm to cm scale) ubiquitous banding of the sulphides is due to variation in the proportion of the various sulphide minerals and is inferred

to be tectonic in origin (S_1). Other accessory minerals, such as marcasite, cobaltite, arsenopyrite, laitakarite, magnetite, native bismuth and paraguanajuatite complete the paragenesis (Marcoux et al., 200X).

Several zones of oxidation are present at surface and these are related to faults and fractures. However, at Sidi M'Barek, a well-developed gossan (up to 20 m thick) is observed, but this area has not been fully explored. Details of the deformational history of the Draa Sfar orebodies as well as details of their mineralogy are described in Marcoux et al. (200X).

4. Geochemistry and hydrothermal alteration

One hundred and twenty-five drill core samples (7 cm in length) were collected from three representative drill holes, DS110, DS132, and DS125. These, plus fifteen surface samples were selected to provide coverage of the entire Draa Sfar deposit, its enclosing host rocks, and related hydrothermal alteration (Fig. 2). The drill core samples were powdered using an agate shatter box at the sample preparation laboratory, Marrakech—Cadi Ayyad University, Morocco.

Major elements (oxides), trace elements and rare-earth elements (REE) were analyzed at Actlabs, Toronto, using a lithium metaborate/tetraborate fusion inductively coupled plasma whole rock and a trace element inductively coupled plasma-mass spectrometer research package (Supplementary Tables 1a,b and c). The fusion process ensures total dissolution of elements that reside in resistant phases. Analyses were performed using Actlab reference standards. All other analytical results and sample locations are available from the first author upon request.

Mineral compositions were determined on a CAMECA SX-50 electronic microprobe in the BRGM/ISTO laboratory, Orléans, France (Table 1a and Table 1b). The quantitative mineralogy of the 125 drill core samples, most of which are petrographically irresolvable, fine-grained argillites and siltstones, was determined by XRD using the Rietveld method at Laurentian University, Sudbury, Canada (Rietveld, 1969).

4.1. Geochemistry of the volcanic and intrusive lithofacies

Lithogeochemistry is a useful tool to determine the chemical composition and magmatic affinity of volcano-plutonic successions (Finlow-Bates and Stumpfl, 1981, Ludden et al., 1982, Lesher et al., 1986, MacLean and Kranidiotis, 1987, Barrett and MacLean, 1994 and Jenner, 1996). Even within mining districts where hydrothermal alteration has severely modified the primary composition of the rocks, it is possible to identify protoliths, and to determine the magmatic affinity of volcanic rocks or the provenance of sedimentary rocks by using immobile and incompatible elements. For example, a number of recent studies (MacLean and Kranidiotis, 1987, Barrett and MacLean, 1999 and Lentz, 1996) have determined that the elements, Al, Ti, Zr, Nb, Y and the heavy rare-earth elements (HREE) are typically immobile during alteration associated with volcanogenic massive sulphide (VMS) and gold deposits. However, the immobility of an element or oxide should never be assumed, but must be demonstrated prior to their use in discrimination diagrams and before calculating compositional gains and losses. In this study, petrographic analysis was the first step in selecting least-altered samples. This was followed by using the alteration index (AI) of Ishikawa et al. (1976); $AI = ((MgO + K_2O) / (MgO + K_2O + Na_2O + CaO)) \cdot 100$ (in wt.%),

where samples with AI outside the range of 35 ± 10 (Laflèche et al., 1992) were considered as altered.

The next step involved plotting selected least-altered samples on binary diagrams using elements with high ionic charge (*e.g.*, high field strength elements, HFSE, REE). If the elements/oxides selected are immobile they should define a best-fit line that has a high Pearson product correlation coefficient (r; Edwards, 1976) and that passes through the origin. Based on this test, binary diagrams for Zr–TiO_2, Nb–Y, Nb–Zr, Zr–La, Zr–Y, and Al–Ti all display a high correlation ($r > 0.9$) indicating that these elements can be considered as immobile in this study.

The range of SiO_2 in the volcanic rocks (65 to 75 wt.%) and the position of the least-altered rocks on a Winchester and Floyd (1977) diagram indicate that rocks are rhyodacitic in composition (Fig. 8a). In addition to SiO_2, the volcanic rocks of the mine area are similar in their alkali content ($Na_2O + K_2O = 3.5\%$) to acidic and intermediate rocks of the Central Jebilet (Aarab, 1995). Based on 2000 analyses from the mine database, the volcanic lithofacies have a higher content of Cu, Pb, Zn, and S than the sedimentary lithofacies.

The aphanitic dikes in the footwall sequence are intermediate in composition, whereas the large gabbro sill in the hanging wall succession has a SiO_2 content that ranges from 46 to 52 wt.% (Fig. 8a; Winchester and Floyd, 1977).

A chondrite-normalized REE diagram, as well as ratios of Zr/Y (mean = 3.13), Y/La (mean = 1.5) and Yb/Th (mean = 0.36), indicate that the volcanic rocks have a tholeiitic affinity (*e.g.*, Barrett and MacLean, 1999; Lentz et al., 1995; Fig. 8 and Fig. 9). The REE profiles for the felsic volcanic/volcaniclastic rocks are identical and display a slight enrichment in the light REE, a pronounced negative Eu anomaly, and a flat heavy REE profile that are typical of FIIIb, tholeiitic, felsic volcanic rocks (Fig. 9; Hart et al., 2004). The parental magmas for FIIIb felsic volcanic rocks are interpreted to have formed by shallow level (low pressure), partial melting of the crust (< 10 km) within a rift environment (Hart et al., 2004), which is consistent with an epicontinental, rift basin geodynamic setting for the Jebilet Massif as proposed by Huvelin (1977), Beauchamp (1984), Aarab and Beauchamp (1987), Piqué and Michard (1989) and Beauchamp et al. (1991). These compositional characteristics are similar to most felsic volcanic and volcaniclastic rocks of the Hercynian Central Jebilet and Guemassa domains (JICA, 2003 and Aarab and Beauchamp, 1987).

4.2. Geochemistry of the sedimentary lithofacies

The sedimentary lithofacies at Draa Sfar are divided into an argillite, carbonaceous argillite–siltstone footwall facies and a carbonaceous argillite–siltstone hanging wall facies that shows a progressive enrichment in carbon and carbonate upwards, culminating with rhythmic layered bioclastic limestones (Fig. 2). Variations in Al, Ti, Zr, Nb, Ni, La, V, Sc and to a lesser extent Si and P, on simple geochemical profiles clearly distinguish the sedimentary lithofacies from the volcanic lithofacies (Fig. 10a, b, c). In particular, the Zr/TiO_2 ratio is an effective tool to distinguish and map the volcanic and sedimentary lithofacies in the mine area, which are often very fine-grained, deformed, variably altered and, consequently, are difficult to distinguish by appearance alone.

The geochemical compositions of fine-grained clastic sedimentary rocks are controlled by: (1) the provenance (terrigeneous source area) of the original sediment; (2) the syndepositional

hydrothermal and hydrogeneous chemical component; and (3) post-depositional, diagenetic, hydrothermal-seawater alteration and metamorphic processes (Lentz et al., 1995 and Lentz, 1996). There is sparse published information on the chemostratigraphy of the Sarhlef volcano-sedimentary succession, the petrogenesis of the volcanic rocks, or the environment of deposition and provenance of the dominantly argillaceous sedimentary strata in the Central Jebilet domain. Based on the abundance of carbonaceous argillite, Beauchamp et al. (1991) considered the Sarhlef succession to reflect an anoxic depositional environment; their work, however, was on strata located outside of the Draa Sfar mine.

Petrographic analysis indicates that the relative proportions of mica, quartz, and feldspar components, as well as carbonate, control the composition of the sedimentary rocks. In order to determine the provenance, original composition and tectonic environment of sedimentary rocks, many workers have used the HFSE: Al, Ga, Ti, Sc, Zr, Hf, Y, LREE, Th, Nb, and Ta to identify the source of sediments (Lentz et al., 1995 and Lentz, 1996). Al_2O_3, in particular, is very useful because most of the trace elements originally adhere to clays and consequently covary with Al_2O_3. Thus, the close geochemical coherence of many trace elements with Al_2O_3, which also behaves as an immobile component, allows examination of the geochemical variation. The systematic variation between Al_2O_3 and SiO_2, K_2O, TiO_2, MnO, CaO, Zr, Y, Cr, Nb, V, Ce and La indicates a pelagic–terrigeneous source for the siliciclastic sediments (Bonatti et al., 1972; *cf*. Lentz et al., 1996). This variation with Al_2O_3 is less evident for MgO, P_2O_5, Na_2O, Fe_{total} and other trace elements probably due to subsequent alteration and/or metamorphism.

A high pelagic component is indicated by Na_2O values > 0.65 on an $Al_2O_3 / (Al_2O_3 + Na_2O + K_2O)$ *versus* Na_2O diagram (Fig. 8c; weathering diagram of Taylor and McLennan, 1985 and Lentz et al., 1995). This high pelagic content is confirmed in Fig. 8d, a plot of Fe/Ti *vs.* Al / (Al + Fe + Mn) (Boström, 1973), which suggests that terrigeneous–pelagic detritus (high Al_2O_3) has been mixed with a minor hydrothermal component (high Fe and Mn).

The Fe/Mn ratio is commonly used to establish the relative oxidation state of sediments (Krauskopf, 1957 and Lentz et al., 1996), where a high Fe/Mn ratio indicates anoxic conditions and a low Fe/Mn ratio indicates oxic conditions. As noted by Lentz et al., 1996 and Lentz et al., 1995 variations in Fe/Mn occur because Mn is more soluble than Fe over a large range of Eh(O_2) and pH (acidity) conditions (Krauskopf, 1957, Maynard, 1983 and Force and Cannon, 1988). As illustrated in Fig. 11, the high Fe/Mn ratio for footwall and hanging wall argillite in the three drill holes is consistent with an anoxic environment as proposed by Beauchamp et al. (1991). Within drill holes DS132 and DS125, there is a pronounced increase in the Fe/Mn ratio (100 and 200) in the footwall argillite upon approaching the massive sulphide and a sharp decrease in this ratio (75) in the hanging wall sedimentary strata. However, in drill hole DS 110, the footwall argillite shows a gradual increase in the Fe/Mn ratio that continues into the hanging wall, with a pronounced spike in the Fe/Mn ratio (150) within a footwall volcaniclastic unit and immediately overlying argillite from 200 to 275 m. The systematic increase in the Fe/Mn ratio toward massive sulphide suggests that the Fe/Mn ratio has been affected by a hydrothermal addition of Fe relative to Mn, under low Eh conditions during formation of the massive sulphide deposit, *i.e.*, fixing Fe relative to Mn during alteration of the footwall volcanic and sedimentary rocks. It is also possible that the footwall argillite and volcaniclastic rocks, particularly those in drill hole 110, were affected by seawater alteration, thus adding Mg at the expense of Fe; an interpretation that is consistent with the lower Fe / (Fe + Mg) of argillite in drill hole 110 relative to the other two

profiles (Fig. 11). Thus, the Fe/Mn ratio of footwall argillite in the three Drill Holes does not reflect the primary paleoenvironment that existed in the immediate footwall to the massive sulphide. Rather, it reflects subsequent alteration during the mineralization event. The high Fe/Mn ratio (50–70) of the hanging wall carbonaceous argillite is relatively constant in the three drill holes and supports an anoxic environment, as does the absence on Mn-rich sediments throughout the Sarhlef series.

5. Hydrothermal alteration

5.1. Mineralogical characteristics and zonation

Alteration was examined using samples collected from outcrops and the three drill holes mentioned previously. Chemical, petrographic, microprobe, and X-ray diffractometry (XRD) analysis (Rietveld method) were performed on the samples (see Fig. 2; Supplementary Tables 1a,b and c). The principal minerals formed by hydrothermal alteration are chlorite and muscovite, with minor quartz and calcite. These minerals are also present in the least-altered volcanic and sedimentary rocks, but the alteration minerals are distinct in their larger grain size, higher modal abundance, and their mapped distribution, which are spatially related to the orebodies (Fig. 12).

There is a clear zonation of alteration mineral assemblages at the deposit scale. In the more proximal volcanic area to the south, argillite, in the immediate footwall to the Tazakourt orebody, is characterized by chlorite alteration (Fig. 12 and Fig. 13). Here, intense chlorite alteration is best developed in strata within 10 m of the massive sulphide orebody, where medium to dark green chlorite is the dominant alteration mineral with minor phengite (XRD) and rare microcrystalline quartz and feldspar (Fig. 13b). Chlorite–quartz veins and pyrite veins occur as irregular lenses along the contacts of the massive sulphide and host sedimentary rocks. The veins display textures and structures typical of syntectonic veins and provide evidence of a later brittle deformation. Tectonic breccias and small-scale faults isolate well foliated and chloritized wall rock fragments (Fig. 13c).

Chloritization is accompanied by the breakdown of feldspar, a decrease in the abundance of muscovite, and a substantial increase in the abundance of calcite and quartz. Dark, Mg-rich chlorite is typical of the chloritized inclusions within the ore (*e.g.*, samples DS220, DS128M5; Table 1a), which also contain up to 40 to 80% talc (see Fig. 6b in Marcoux et al., 200X). Primary textures and mineralogy are poorly preserved in the chloritized, talc-altered inclusions, but the protolith is interpreted to be the argillite–siltstone lithofacies. XRD analysis indicates that away from the massive sulphide lens the feldspar is dominantly albite with rare andesine or orthoclase, whereas chlorite varies from clinochlore to chamosite with increasing distance from ore (Fig. 14).

The alteration assemblage in the immediate hanging wall strata to the Draa Sfar deposit differs from the chlorite alteration assemblage within the footwall to the Tazakourt orebody. Along the entire hanging wall of the Draa Sfar orebody the argillite is characterized by enrichment in muscovite (50 to 70%), quartz (10 to 20%), chlorite (5 to 8%), calcite (2 to 4%), and fine opaque minerals that collectively define a sericite zone.

In the more volcanically distal, northern part of the deposit, alteration within the footwall argillaceous sedimentary rocks is characterized by an increase in the abundance of muscovite relative to chlorite (Fig. 12c). The hanging wall alteration is similar to that in the south and

the sedimentary rocks are dominated by a quartz–muscovite assemblage that passes progressively upwards into a quartz–calcite–muscovite assemblage. Thus, the alteration mineral assemblages, their abundance, and their distribution indicate a hanging wall sericite alteration along the length of the deposit and a footwall alteration that is dominated by chlorite to the south (Tazakourt) and sericite to the north (Sidi M'Barek).

In addition, the higher proportion of argillite *versus* carbonaceous argillite within the immediate deposit footwall *versus* equivalent strata located outside of the deposit area, and the localized "bleaching" of footwall carbonaceous sedimentary rocks, suggests organic carbon has been removed by temperature-sensitive hydrothermal methanogenic reactions $2H_2O + C \rightarrow CH_4 + O_2$ (and $CO_2 + 2H_2$) responsible for variable H_2O–CH_4–CO_2 that would impart a very low $f(O_2)$ (high CH_4/CO_2) during alteration. Very low $f(O_2)$ conditions during alteration are consistent with the particularly anoxic conditions required to form primary pyrrhotite, the dominant Fe-sulphide at Draa Sfar.

5.2. Mineral compositions

The composition of chlorite, muscovite and plagioclase from hydrothermally altered and least-altered sedimentary rocks was determined using an electron microprobe in order to determine possible compositional differences in these minerals in samples collected across the deposit.

Chlorite composition was determined for twelve samples (61 point analyses) representing a profile across the orebody (see Fig. 2 and Table 1a), including samples of chloritized wall rock fragments within the massive sulphide (*e.g.*, DS220). Chlorite displays a spectrum of compositions from daphnite–ripidolite within argillites and volcanic rocks outside of the footwall chlorite alteration zone (least altered), to clinochlore within the chlorite alteration zone and within chloritized inclusions inside the orebody (Fig. 14). Chlorite in the chlorite alteration zone is more magnesian (> 15 wt.% MgO,< 25 wt.% FeO) than chlorite from less altered rocks (< 14 wt.% MgO, > 25 wt. FeO). The $Fe_{total} / (Fe_{total} + Mg)$ ratio ranges from 0.3 to 0.95. The higher Mg content of chlorite in the footwall alteration zone and within chloritized inclusions in the massive sulphide is indicative of intense Mg-metasomatism that accompanied sulphide deposition.

Slack and Coad (1989) and Kranidiotis and MacLean (1987) adapted and used the chlorite geothermometer of Cathelineau and Nieva (1985) to determine the formation temperature (*T*, degrees Celsius) based on the concentration of tetrahedral Al (Al^{iv}) in chlorite:

$$T = 106Al^{iv} + 18$$

(Slack and Coad, 1989)

In this equation the Al^{iv} values must first be corrected by adding $0.7[(Fe / (Fe + Mg)_{chl}]$. The equation is applicable to the chlorites that lie on an Al-saturation boundary, such as the chlorites at Draa Sfar (not illustrated). The use of the geothermometer for our samples (Table 2) with three different Mg compositions (Fig. 14) yields temperatures of 376 to 388 °C for chlorite (Fe-rich) in least-altered volcanic rocks and argillite, temperatures of 322 to 375 °C for chlorite in altered footwall argillite, and temperatures of 276 to 346 °C for chlorite (Mg-rich) within wall rock fragments inside the massive sulphide and in altered argillite immediately adjacent to massive sulphide. The higher temperature indicated for chlorite in

least-altered argillite *versus* chlorite within altered argillite is not consistent with a primary hydrothermal temperature regime in which the chlorite in the altered argillite would be expected to have formed at higher temperatures than "background" chlorite in least-altered argillite. The lower temperature for hydrothermal chlorite in altered argillite proximal to the deposit may indicate metamorphic resetting or, perhaps, that chlorite within and below the Draa Sfar deposit formed by the continued influx of advecting seawater proximal to the deposit?

Muscovite represents the second principal phyllosilicate in altered and least-altered rocks; analyses of muscovite from fifteen samples (66 point analyses) are given in Table 1b. Muscovite contains trace amounts of Ti, insignificant amounts of Cr, V, Zn and Mn (0.1 to 0.2%) and up to 4.5% H_2O (computed) and shows a change in composition to lower Fe and Mg, and high K content, with increasing distance from the orebody (Fig. 15).

Plagioclase adjacent to the chlorite alteration zone and more distal to the deposit, in both volcanic and sedimentary rocks, is consistently pure albite ($> 99_{Ab}$). *Biotite* is uncommon, but where present is retrograded to chlorite; this indicates that the rocks reached a metamorphic grade of upper greenschist facies during prograde metamorphism M_1.

5.3. Compositional changes and mass balance calculations

In order to ascertain the geochemical variations surrounding the Draa Sfar deposit the untreated geochemical data for holes DS110, DS125, and DS132 are plotted as a function of depth and spatial relationship to the deposit in Fig. 10a, b, c. The variation in SiO_2, MnO, Fe_2O_{3T}, MgO, K_2O, and CaO indicates that they were relatively mobile during wall rock alteration reactions. FeO_t + MgO may be grouped together as a unique chlorite component, whereas CaO and Na_2O can be grouped as a plagioclase or alkalies component. Similarly, K_2O may be considered as a muscovite component, whereas Al_2O_3 is an immobile component that is also common to micas and feldspars. From Fig. 10 it is apparent that CaO and Na_2O decrease sharply relative to other components in the chlorite alteration zone and probably represent plagioclase destruction as indicated by the XRD data. The increase of Fe and Mg within the chlorite alteration zone and toward the orebody, a common trend in chlorite alteration zones associated with VMS deposits (Fig. 11; Riverin and Hodgson, 1980, Galley, 1995, Galley et al., 1995 and Lentz et al., 1997), corresponds to the measured increase in the abundance of chlorite. K_2O shows a contrasting distribution between the footwall alteration zones of the southern, Tazakourt and the northern, upper Sidi M'Barek orebodies. K_2O decreases within the chlorite alteration zone of the Tazakourt orebody, but increases within the footwall alteration zone to the upper Sidi M'Barek orebody. This mimics the variation in modal abundance of chlorite and sericite determined through XRD and clearly defines a lateral transition form a chlorite-dominated footwall alteration zone below the Tazakourt orebody to a sericite-dominated alteration zone below the upper Sidi M'Barek orebody.

The intensity of alteration can also be monitored by using alteration indices (Fig. 11) that are based on cation ratios, such as the alkali alteration index, 3K/Al (representing K-mica), and the Na/Al index (representing albite). These variables generally show antipathetic trends between the Tazakourt and Sidi M'Barek orebodies, consistent with the observed chemical and mineralogical changes. The (Fe + Mg) / Al and (Fe + Mg) / (Na + K) indices have been used to monitor chlorite alteration in VMS systems (Riverin and Hodgson, 1980 and Galley et al., 1995). At Tazakourt these indices increase toward the footwall chlorite alteration zone,

whereas at Sidi M'Barek pervasive sericite alteration in the footwall to the upper orebody negates the usefulness of this alteration index (Fig. 11a, b).

The isocon method of Grant (1986) has been used to assess the flux of components as gains (positive) or losses (negative) from least-altered to more-altered rocks. The selection of the isocon for each case is based on the best-fit line for components shown to be immobile in this study, such as Ti, Zr, Nb, Y and Al. In the footwall to Tazakourt (Hole DS110), mass balance calculations of chloritic proximal alteration in the volcaniclastic rocks relative to least-altered equivalents indicate a marked enrichment in Fe, Mg, V and depletion of K, Ca, Na, Ba, Be, Bi and Nb with chlorite alteration. Losses in K and gains in Mg and Fe account for the relative decrease of sericite and enrichment in chlorite. Like the volcaniclastic rocks, the footwall argillites show the same gains and losses for Fe, Mg, K, and Ca with chloritization (Fig. 16). Si addition in both rock types is minor.

In the sericitic footwall to upper Sidi M'Barek orebody (Hole DS125) the altered sediments plotted against the least-altered precursor indicate minimal mass change. The major elements Fe_{total}, Na, P, Al, Si, and Mn and trace elements S, Cu, Th, Sr, Yb, Zr, Cr, and Nb define the isocon line (Fig. 16d). Potassium, Mg, Rb, Y, Ni and La are added, whereas Pb and Ga are lost, which is consistent with compositional changes associated with sericite alteration.

The footwall chlorite and sericite alteration zones have a morphology that is best described as stratabound or semiconformable. No discordant, deep penetrating alteration and sulphide stringer zone has been recognized to date below either of the massive sulphide orebodies. This is not unexpected as sediment-hosted massive sulphide deposits, like Draa Sfar, are characterized by diffuse, broad, footwall alteration zones and poorly developed stringer sulphides (Gibson, 2005 and Franklin et al., 2005). However, because of the pronounced deformation within the entire belt and at Draa Sfar in particular, the semiconformable nature of the footwall alteration may, in part, reflect transposition during D_1. Structural transposition would make it difficult to recognize a discordant alteration zone, especially if one considers that there a very few drill holes that extend deep into the footwall rocks.

In DS125, the abundance of Pb, Zn, and Cu are considerably lower in the altered footwall argillite relative to the least-altered argillite and hanging wall argillite; the depletion in base–metal abundances is coincident with the Na depletion zone. However, in DS132 the Pb abundance is lower throughout the section, with irregular Zn values, and consistently increasing Cu contents (up to 910 ppm), but then decreases near the ore zone. In DS110, Pb is relatively low throughout the section, but Cu increases to 100 ppm and Zn increases to 223 ppm, then decreases as the ore horizon is approached. It appears that footwall zones enriched in Cu and Zn are coincident with S enrichment as well as zones of chloritization; it is possible they represent cryptic upflow zones in the footwall sedimentary sequence, although their morphology may be deformed and transposed.

The metal zoning within the Draa Sfar deposit at first appears inconsistent with the overall alteration pattern of chlorite to the south and sericite to the north as the most Cu-rich mineralization occurs at Sidi M'Barek and not at Tazakourt. However, it is the upper or western sulphide lens at Sidi M'Barek that is correlated with the Tazakourt orebody and the Zn-rich rich character of this upper lens (6 to 7% Zn, 0.3% Cu) is consistent with the overall deposit-scale metal and alteration zoning at this time-stratigraphic interval. The reason for the Cu-rich character (2 to 3% Cu, 0.3% Zn) of the stratigraphically lower, eastern sulphide lens at Sidi M'Barek is uncertain. It may be related to the overlying Zn-rich lens, or it could be part

of a new, unrelated lens that has been structurally dislocated. There is not enough geological (drill hole) data at this time to make a reasonable interpretation.

6. Discussion and conclusions

The dominance of more than 1 km of black, carbonaceous argillites within the footwall and hanging wall strata to the Draa Sfar deposit suggests that it formed within a restricted, sediment-starved, anoxic basin within the upper part of the Sarhlef Formation (*e.g.*, Beauchamp et al., 1991). The argillites formed through background suspension sedimentation within the basin whereas the siltstones, which noticeably lack carbon, are distal turbidites that were derived from the basin margins. This interpretation is consistent with the particularly low fO_2 conditions required to form primary pyrrhotite, the dominant Fe-sulphide mineral at Draa Sfar (Marcoux et al., 200X). Although deformation has obscured the contacts between the Draa Sfar deposit and its argillaceous host rocks it is likely that it formed at and below the seafloor within anoxic, pelagic muds as proposed by Marcoux et al. (200X), and as also proposed for the Hajar massive sulphide deposit by Leblanc (1993). The interpretation that inclusions of talc- and chlorite-rich altered argillite within the massive sulphide may be structurally dismembered beds of inter-sulphide argillite also supports a sub-seafloor replacement origin.

The occurrence of a proximal, rhyodacitic flow-dome complex and associated, coarse volcaniclastic lithofacies below the Tazakourt orebody suggests that the basin developed above or contained a local, felsic volcanic centre. Once unfolded, the increase in thickness of the argillaceous sediments to the north, off the flank of the rhyodacitic flow/dome complex, suggests that the felsic centre was localized along synvolcanic/sedimentary faults that may, in part, define the south limit of the Draa Sfar basin (Fig. 17). Thin, felsic volcaniclastic beds intercalated with argillite in the footwall to the Tazakourt orebody may have been derived from mass wasting or pyroclastic eruptions that accompanied emplacement and growth of the rhyodacitic domes; alternatively, they may have been derived from a contemporaneous, but more distal volcanic centre.

Carbonaceous argillite within the hanging-wall to both the Tazakourt and Sidi M'Barek orebodies shows a clear change in mineral assemblage with less chlorite and more sericite and calcite compared to the footwall sequence. The carbonaceous hanging-wall sequence has been interpreted as representing a shallowing upward sequence in the Jebilet Basin (*cf*. Bernard et al., 1988). This is consistent with the presence of carbonate units located stratigraphically higher in this sequence.

The development of a crudely stratabound, chlorite–sericite alteration zone within the footwall to the Draa Sfar deposit undoubtedly reflects some transposition during deformation, but is also characteristic of alteration zones associated with volcaniclastic or sediment hosted volcanogenic massive sulphide deposits (Gibson et al., 1999, Gibson, 2005 and Franklin et al., 2005). Chlorite alteration zones represent the higher temperature, primary hydrothermal conduit in most VMS deposits (MacGeehan, 1977, Riverin and Hodgson, 1980, Franklin et al., 1981, Kranidiotis and MacLean, 1987, Galley, 1995 and Franklin et al., 2005). The lateral change from predominantly chlorite alteration in the footwall to the Tazakourt orebody to sericite in the south, below the Sidi M'Barek orebody correlates with a change in the footwall from a proximal volcanic environment to a more distal volcanic environment. Localized zones of Cu and Zn enrichment within chloritized argillite and near the base of the Tazakourt massive sulphide lens in drill Holes DS110 and 132 may define cryptic upflow zones that

were subsequently deformed and transposed. The occurrence of intensely chloritized and talcose inclusions of argillite in the massive sulphide at Tazakourt would also be expected to form within an upflow zone where argillite intercalated with massive sulphide in a seafloor or sub-seafloor environment would be altered and replaced by chlorite and talc. The chlorite–talc stability plot of Kharaka and Barnes (1973) (see also Roberts and Reardon, 1978 and Zierenberg and Shanks, 1994) illustrates that the formation of talc relative to chlorite is also favoured by higher temperatures, higher activities of magnesium, and lower aluminum activities at the discharge sites. This indicates the importance of both Mg-metasomatism nearer the chlorite core of the hydrothermal discharge system and the role of synvolcanic structures in controlling the location of coincident volcanic and hydrothermal vents. Fig. 17 shows the distribution of sulphide ore and the relationship between volcano-sedimentary lithofacies and the alteration zones; this diagram is based on data from numerous E–W-oriented drill holes. Thickness variations of the sulphide lens (0 to 30 m) are probably related to primary topography within the basin and subsequent deformation.

The presence of pronounced footwall chlorite (sericite) and hanging wall sericite alteration zones, along with the spatial and temporal association of the Draa Sfar deposit with proximal volcanism and possible synvolcanic/synsedimentary structures are all features that are more consistent with volcanogenic massive sulphide deposits (VMS) and not sedimentary exhalative deposits (SEDEX). The heat engine required to initiate and sustain the long-lived, high temperature hydrothermal system responsible for the formation of the Draa Sfar and other VMS deposits in the Jebilet and Guemassa massifs is interpreted to be mantle-derived, magmatic heat that was confined in space and time to rifting and the formation of a rift-basin that was infilled with sedimentary and lesser volcanic rocks of the Sarhlef volcano-sedimentary succession. The numerous gabbro sills within the Sarhlef have been interpreted as a manifestation of mantle–magmatism and heat that accompanied rifting and sedimentation (Gibson et al., 2005). The high-temperature and low pressure conditions required to form FIIIb felsic volcanic rocks, such as those at Draa Sfar, support their generation by partial melting of the crust at a shallow crustal level within a rift environment where partial meting occurred due to the anomalously high heat flow associated with the upwelling of hot mantle into thinned, rifted crust (Hart et al., 2004).

Using the lithotectonic classification of Franklin et al. (2005), the Draa Sfar deposit would fall in the siliciclastic–felsic type that consists of two distinct lithofacies, a siliciclastic lithofacies composed predominately of wacke, sandstone, siltstone, argillite and locally iron formation or Fe–Mn-rich argillite, and a pelitic lithofacies facies composed predominately of argillite, carbonaceous argillite, marl, and carbonate units (bioclastic and chemical). The Draa Sfar deposit would be grouped in the pelitic lithofacies, whereas other siliciclastic–felsic VMS deposits, such as some of the IPB deposits and deposits of the Bathurst district, would fall in the siliciclastic lithofacies association.

In fact, VMS deposits of the Jebilet and Guemassa massifs have been compared to those of the IPB, based on their similar age and inferred geodynamic environment (Bordonaro et al., 1979, Bernard et al., 1988 and Lescuyer et al., 1998). However, there are distinct differences between these two VMS districts, such as: (1) although many IPB VMS deposits are hosted by carbonaceous argillite, especially those along the southern margin of the IPB (*e.g.*, Tharis), the Draa Sfar and other VMS deposits in the Moroccan Mesta differ in that they occur within a thick sedimentary succession (> 1 km) dominated by carbonaceous, pelagic sediments; (2) unlike the IPB deposits the Moroccan deposits are not associated with Mn-rich sediments (exhalites); (3) pyrrhotite is the dominant, primary Fe-sulphide in the Moroccan deposits

compared to pyrite in the IPB deposits; and (4) footwall alteration associated with the Moroccan VMS deposits is characterized by a well developed chlorite alteration, whereas footwall alteration associated with IPB VMS deposits is characterized by sericite (Lescuyer et al., 1998, Brunet et al., 2004 and Gibson et al., 2005). These differences may reflect a more sediment-starved, restricted, and anoxic environment at Draa Sfar and for other VMS deposits in the western Moroccan Meseta.

Acknowledgements

This research would not have been possible without the financial support of REMINEX. In particular we would like to thank Solange Brunet for her time, effort and guidance. Dr Andrew McDonald, MERC, Laurentian University, provided the excellent XRD analysis and modal analysis using the Rietveld method. Thorough and helpful reviews by Ore Geology Reviews reviewers Rodney Allen and Fernando Tornos and a subsequent review by Philips Thurston improved the manuscript. H.L Gibson gratefully acknowledges the financial support of an NSERC discovery grant.

References

Aarab, 1995 Aarab, E.l., 1995. Genèse et differentiation d'un magma tholeitique en domaine extensif intracontinental: l'exemple du magmatisme pre-orogenique des Jebilet (Maroc Hercynien). Unpublished thesis, Cadi Ayyad University, Marrakesh, Morocco, 253 pp.

Aarab and Beauchamp, 1987 E.l. Aarab and J. Beauchamp, Le magmatisme carbonifère pré-orogénique des Jebilet centrales (Maroc). Précisions pétrographiques et sédimentaires. Implications géodynamiques, *Comptes Rendus de l'Académie des Sciences Paris (Série II)* **304** (1987), pp. 169–175.

Barrett and MacLean, 1994 T.J. Barrett and W.H. MacLean, Mass changes in hydrothermal alteration zones associated with VMS deposits of the Noranda area, *Exploration and Mining Geology* **3** (1994), pp. 131–160.

Barrett and MacLean, 1999 T.J. Barrett and W.H. MacLean, Volcanic sequences, lithogeochemistry, and hydrothermal alteration in some bimodal volcanic-associated massive sulphide systems, *Reviews in Economic Geology* **8** (1999), pp. 101–131.

Beauchamp, 1984 J. Beauchamp, Le Carbonifère inférieur des Jebilet et de l'Atlas de Marrakech (Maroc): Migration et comblement d'un bassin marin, *Bulletin Société Géologique de France* **7-XXVI-6** (1984), pp. 1025–1032.

Beauchamp et al., 1991 J. Beauchamp, A. Izart and A. Piqué, Les bassins d'avant-pays de la chaîne hercynienne au Carbonifère inférieur, *Canadian Journal of Earth Sciences* **28** (1991), pp. 2024–2041.

Bernard et al., 1988 A.J Bernard, O.W. Maier and A. Mellal, Aperçu sur les amass sulfurés massifs des hercynides marocaines, *Mineralium Deposita* **23** (1988), pp. 104–114.

Bonatti et al., 1972 E. Bonatti, T. Kraemer and H. Rydell, Classification and genesis of submarine iron–manganese deposits. In: D. Horn, Editor, *Ferromanganese deposits from the ocean floor, Symposium volume*, Columbia University (1972), pp. 149–165.

Bordonaro, 1983 M. Bordonaro, Tectonique et pétrographie du district à pyrrhotite de Kettara (Paléozoïque des Jebilet, Maroc), *Thèse 3ème cycle*, Université Louis Pasteur de Strasbourg (1983) 132 pp.

Bordonaro et al., 1979 M. Bordonaro, J.L. Gaillet and A. Michard, Le géosynclinal carbonifère sud-mésétien dans les Jebilet (Maroc); une corrélation avec la province pyriteuse du sud de l'Espagne, *Compte Rendus Académie Sciences Paris* **288-D** (1979), pp. 1371–1374.

Boström, 1973 K. Boström, The origin and fate of ferromanganoan active ridge sediments, *Stockholm Contributions in Geology* **27** (1973), pp. 147–243.

Brunet et al., 2004 S. Brunet, M. Labriki, A. Mellal and A. Belkabir, Les minéralisations à sulfures massifs de la région de Marrakech, Maroc: contexte géologique et exploration, *Colloque ACFAS* **vol. 72**, Les deuxièmes Journées de Launay, Montreal (2004), p. 23 Abstract volume.

Cathelineau and Nieva, 1985 M. Cathelineau and D. Nieva, A chlorite solid solution geothermometer: the Los Azufres (Mexico) geothermal system, *Contributions to Mineralogy and Petrology* **91** (1985), pp. 235–244.

Edwards, 1976 A.L. Edwards, *An Introduction to Linear Regression and Correlation*, W.H. Freeman, San Francisco (1976) 213 pp..

Essaifi et al., 2004 A. Essaifi, R. Capdevila, S. Fourcade, J.L. Lagarde, M. Ballèvre and C. Marignac, Hydrothermal alteration, fluid flow and volume change in shear zones: the layered mafic–ultramafic Kettara intrusion (Jebilet Massif, Variscan belt, Morocco), *Journal of Metamorphic Geology* **22** (2004), pp. 25–43.

Finlow-Bates and Stumpfl, 1981 T. Finlow-Bates and E.F. Stumpfl, The behaviour of so-called immobile elements in hydrothermally altered rocks associated with volcanogenic submarine–exhalative ore deposits, *Mineralium Deposita* **16** (1981), pp. 319–328.

Fisher, 1966 R.V. Fisher, Mechanism of deposition from pyroclastic flows, *American Journal of Science* **264** (1966), pp. 287–298.

Force and Cannon, 1988 E.R. Force and W.F. Cannon, Depositional model for shallow-marine manganese deposits around black-shale basins, *Economic Geology* **83** (1988), pp. 93–117.

Franklin et al., 2005 J.M. Franklin, H.L. Gibson, I.R. Jonasson and A.G. Galley, Volcanogenic massive sulphide deposits, *Economic Geology 100th Anniversary* **vol 523–560** (2005).

Franklin et al., 1981 J.M. Franklin, J.W. Lydon and D.F. Sangster, Volcanic-associated massive sulphide deposits, *Economic Geology 75th Anniversary* **vol 485–627** (1981).

Galley, 1995 A.G. Galley, Target vectoring using lithogeochemistry: applications to the exploration for volcanic-hosted massive sulphide deposits, *Canadian Institute of Mining and Metallurgy Bulletin* **88** (1995) (990), pp. 15–27.

Galley et al., 1995 A.G. Galley, D.H. Watkinson, I.R. Jonasson and G. Riverin, The subsea-floor formation of volcanic-hosted massive sulphide: evidence from the Ansil deposit, Rouyn-Noranda, Canada, *Economic Geology* **90** (1995), pp. 2006–2017.

Gibson, 2005 H.L. Gibson, Volcano-hosted ore deposits. In: J. Marti and G.G.J. Ernst, Editors, *Volcanoes and the Environment*, Cambridge University Press (2005), pp. 333–386.

Gibson et al., 2005 H.L. Gibson, S. Brunet, A. Belkabir, D. Lentz and E. Marcoux, The spectrum of volcano-sedimentary environments hosting volcanogenic massive sulphide deposits of the Visean, Jebilet and Guemassa Terrains, Morocco, *Canadian Institute of Mining and Metallurgy, Annual Meeting, Toronto, Ontario, Program with Abstracts* (2005), p. 28.

Gibson et al., 1999 H.L. Gibson, R. Morton and G. Hudak, Submarine volcanic processes, deposits and environments favourable for the location of volcanic-associated massive sulphide deposits, *Reviews in Economic Geology* **8** (1999), pp. 13–51.

Grant, 1986 J.A. Grant, The isocon diagram: a simple solution to Gresens' equation for metasomatic alteration., *Economic Geology* **80** (1986), pp. 1976–1982.

Hart et al., 2004 T. Hart, H.L. Gibson and C.M. Lesher, Trace element geochemistry and petrogenesis of felsic volcanic rocks associated with volcanogenic Cu–Zn–Pb massive sulfide deposits, *Economic Geology* **99** (2004), pp. 1003–1013

Hey, 1954 M.H. Hey, A new review of the chlorites, *Mineralogical Magazine* **30** (1954), pp. 277–292.

Huvelin, 1977 P. Huvelin, Etude géologique et gîtologique du Massif hercynien des Jebilet (Maroc occidental), *Notes Mémoires Services Géologiques Maroc* **232bis** (1977) 307 pp.

Ishikawa et al., 1976 Y. Ishikawa, T. Sawagushi, S. Iwaya and M. Horiuchi, Delineation of prospecting targets for Kuroko deposits based on modes of volcanism of underlying dacite and alteration halos, *Mining Geology* **26** (1976), pp. 105–117.

Jenner, 1996 G.A. Jenner, Trace element geochemistry of igneous rocks; geochemical nomenclature and analytical geochemistry. In: D.A. Wyman, Editor, *Trace Element Geochemistry of Volcanic Rocks: Applications for Massive Sulphide Exploration*, *Geological Association of Canada Short Course Notes* **12** (1996), pp. 51–77.

JICA, 2003 JICA, *Report on The Mineral Exploration in Marrakech-Tekna Area Kingdom of Morroco. Phase 1. March 2003. Japan International Cooperation Agency* (2003) 247 pp.

Kharaka and Barnes, 1973 Y.K. Kharaka and I. Barnes, SOLMNEQ—solution–mineral equilibrium computations: U.S. Geological Survey Computer Contribution, *National Technical Information Service* **PB-215 899** (1973) 81 pp.

Kranidiotis and MacLean, 1987 P. Kranidiotis and W.H. MacLean, Systematics of chlorite alteration at the Phelps Dodge massive sulphide deposit, Quebec, *Economic Geology* **82** (1987), pp. 1898–1911.

Krauskopf, 1957 K.B. Krauskopf, Separation of manganese iron in sedimentary processes, *Geochemica et Cosmochimica Acta* **19** (1957), pp. 61–81.

Laflèche et al., 1992 M.R. Laflèche, C. Dupuy and H. Bougault, Geochemistry and petrogenesis of Archean mafic volcanic rocks of the southern Abitibi belt, Québec, *Precambrian Research* **57** (1992), pp. 207–241.

Lagarde and Choukroune, 1982 J.L. Lagarde and P. Choukroune, Cisaillement ductile et granitoides syntectoniques: l'exemple du massif hercynien des Jebilet (Maroc), *Bulletin de la Société Géologique de France* **24** (1982) (2), pp. 299–307.

Leblanc, 1993M. Leblanc, Amas sulfuré formé par injection des sills dans des sédiments. Exemple d'Hajar -Marrakech, Maroc), *Comptes Rendus de l'Académie des Sciences Paris* **316** (1993), pp. 499–504.

Lentz, 1996 D.R. Lentz, Trace-element systematics of felsic volcanic rocks associated with massive-sulphide deposits in the Bathurst Mining Camp: petrogenetic, tectonic and chemostratigraphic implications for VMS deposits. In: D.A. Wyman, Editor, *Trace Element Geochemistry of Volcanic Rocks: Applications for Massive Sulphide Exploration*, *Geological Association of Canada, Short Course Notes* **12** (1996), pp. 359–402.

Lentz et al., 1996 D.R. Lentz, W.D. Goodfellow and E. Brooks, Chemostratigraphy and depositional environment of an Ordovician sedimentary section across the Miramichi-Tetagouche Group contact, northeastern New Brunswick, *Atlantic Geology* **32** (1996), pp. 101–122.

Lentz et al., 1995 D.R. Lentz, S.R. McCutcheon and J.A. Walker, Preliminary geochemical interpretation of metalliferous sedimentary rocks in the Miramichi Anticlinorium, New Brunswick. In: S.A. Merlini, Editor, *Current Research 1994. New Brunswick Department of Natural Resources and Energy, Minerals and Energy Division, Miscellaneous Report* **18** (1995), pp. 91–111.

Lentz et al., 1997 D.R. Lentz, D.C. Hall and L.D. Hoy, Chemostratigraphy, alteration, and oxygen isotope trends in a drillhole profile through the Heath Steele B Zone deposit stratigraphic sequence, New Brunswick, *The Canadian Mineralogist* **35** (1997), pp. 841–874.

Lesher et al., 1986 C.M. Lesher, A.M. Goodwin, I.H. Campbell and M.P. Gorton, Trace element geochemistry of ore-associated and barren, felsic metavolcanic rocks in the Superior province, Canada, *Canadian Journal of Earth Sciences* **23** (1986), pp. 222–237.

Lescuyer et al., 1998 J.L. Lescuyer, J.M. Leistel, E. Marcoux, J.P. Milesi and D. Thieblemont, Late Devonian–Early Carboniferous peak sulphide mineralization in the Western Hercynides, *Mineralium Deposita* **33** (1998), pp. 208–220.

Ludden et al., 1982 J.N. Ludden, L. Gélinas and P. Trudel, Archean metavolcanics from the Rouyn-Noranda district, Abitibi Greenstone belt, Québec. 2. Mobility of trace elements and petrogenetic constraints, *Canadian Journal of Earth Sciences* **19** (1982), pp. 2276–2287.

MacGeehan, 1977 P.J. MacGeehan, The geochemistry of altered volcanic rocks at Matagami, Quebec: a geothermal model for massive sulphide genesis, *Canadian Journal of Earth Sciences* **15** (1977), pp. 551–570.

MacLean and Kranidiotis, 1987 W.H. MacLean and P. Kranidiotis, Immobile elements as monitors of mass transfer in hydrothermal alteration: Phelps Dodge massive sulphide deposit, Matagami, Quebec, *Economic Geology* **82** (1987), pp. 951–962.

Marcoux et al., 200X Marcoux, E., Belkabir, A., Gibson, H., Lentz, D., 200X. Draa Sfar: a Hercynian pyrrhotite–Zn–Cu–Pb ore deposit in the Jebilet, Morocco. Mineralogy, geochemistry and deformation as constrains for a genetic model features. Ore Geology Reviews.

Maynard, 1983 J.B. Maynard, Geochemistry of Sedimentary Ore Deposits, Springer-Verlag, New York (1983) 305 pp.

Nakamura, 1974 N. Nakamura, Determination of REE, Ba, Fe, Mg, Na, and K in carbonaceous and ordinary chondrites, *Geochimica et Cosmochimica Acta* **38** (1974), pp. 757–775.

Piqué and Michard, 1989 A. Piqué and A. Michard, Moroccan Hercynides. A synopsis. The Paleozoic sedimentary and tectonic evolution at the northern margin of West Africa, *American Journal of Science* **29** (1989), pp. 286–330.

Prior et al., 1999 G.J. Prior, H.L. Gibson, D.H. Watkinson, R.E. Cook and M.D. Hannington, Rare Earth and high field strength element geochemistry of the Kidd creek rhyolites, Abitibi Greenstone Belt, Canada: evidence for Archean felsic volcanism and volcanogenic massive sulphide ore formation in an Iceland-Style rift environment. In: M.D. Hannington and C.T. Barrie, Editors, *Economic Geology Monographss* **vol. 10** (1999), pp. 457–484.

Roberts and Reardon, 1978 R.G. Roberts and E.J. Reardon, Alteration and ore-forming processes at Mattagami Lake Mine, Quebec, *Canadian Journal of Earth Sciences* **15** (1978), pp. 1–21.

Rietveld, 1969 H.M. Rietveld, A profile refinement method for nuclear and magnetic structures, *Journal of Applied Crystallography* **2** (1969), pp. 65–71

Riverin and Hodgson, 1980 G. Riverin and J. Hodgson, Wall-rock alteration at the Millenbach Cu–Zn mine, Noranda, Quebec, *Economic Geology* **75** (1980), pp. 424–444.

Slack and Coad, 1989 J.F. Slack and P.R. Coad, Multiple hydrothermal and metamorphic events in the Kidd Creek volcanogenic massive sulphide deposit, Timmins, Ontario: evidence from tourmalines and chlorites, *Canadian Journal of Earth Sciences* **26** (1989), pp. 694–715.

Taylor and McLennan, 1985 St.R. Taylor and S.M. McLennan, The Continental Crust: Its Composition and Evolution, Blackwell Scientific Publications, Oxford (1985) 312 pp..

Winchester and Floyd, 1977 J.A. Winchester and P.A. Floyd, Geochemical discrimination of different magma series and their differentiation products using immobile elements, *Chemical Geology* **20** (1977), pp. 325–343.

Zierenberg and Shanks, 1994 R.A. Zierenberg and W.C. Shanks, Sediment alteration associated with massive sulphide formation in Escanaba Trough, Gorda Ridge: the importance of seawater mixing and magnesium metasomatism, *U.S. Geological Survey Bulletin* **2022** (1994), pp. 257–277.

Figures

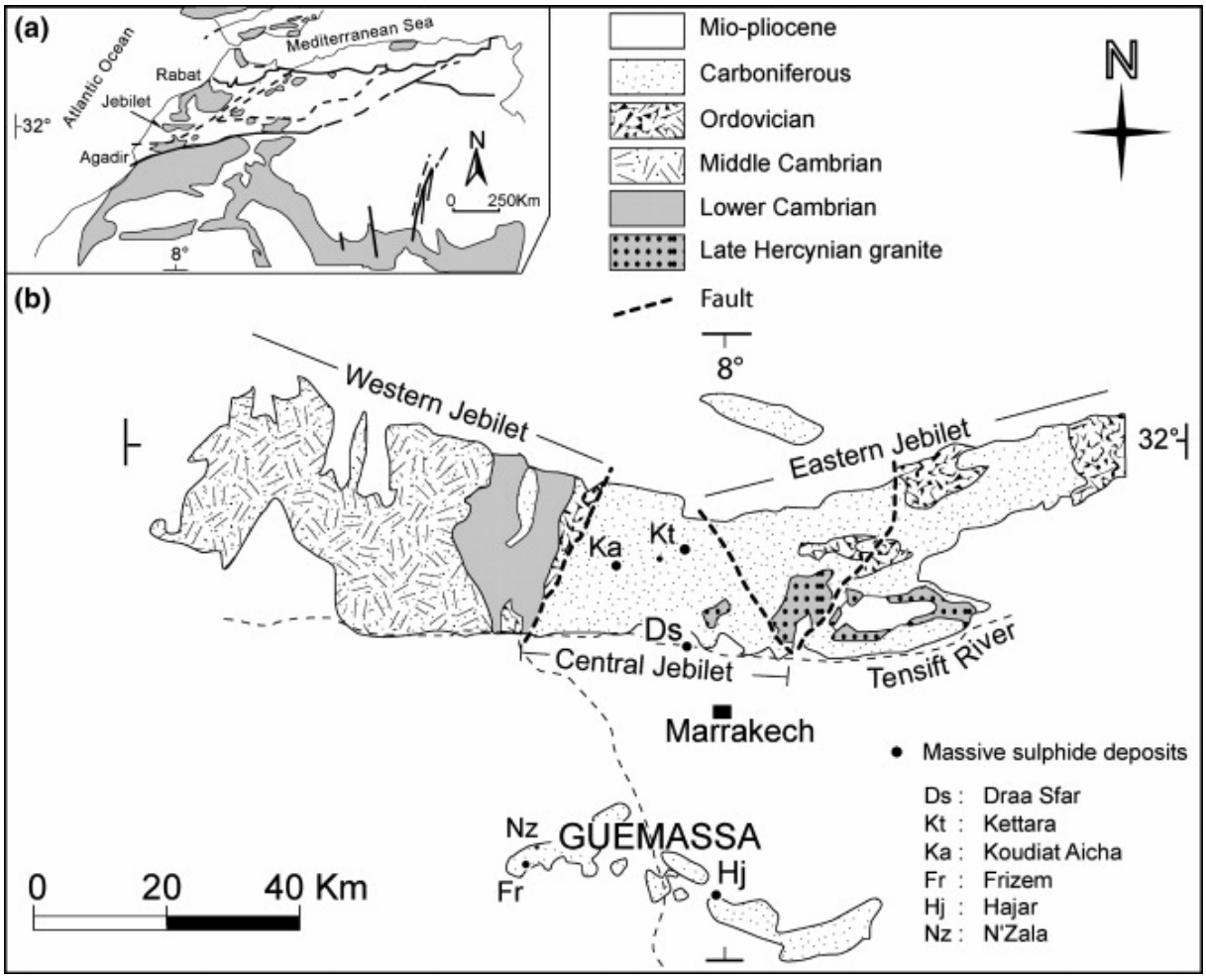

Fig. 1. (a) The Jebilet massif in the framework of the Paleozoic outcrops of North Africa (in grey). (b) General geological map of the Hercynian Jebilet and Guemassa massifs showing the location of the principal massive sulphide deposits (modified from Huvelin, 1977).

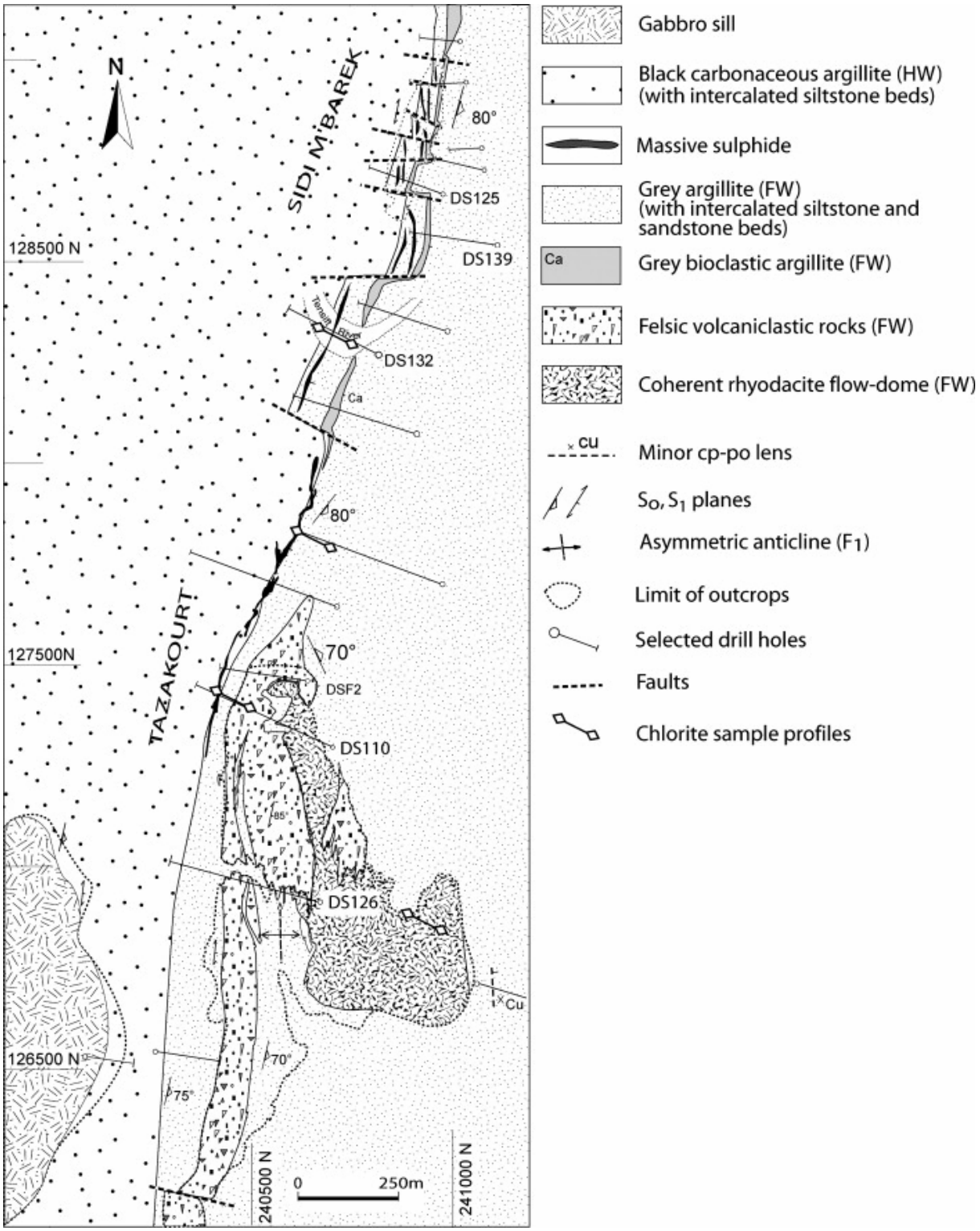

Fig. 2. Geological map of the Draa Sfar mine area showing the surface projection of the Tazakourt and Sidi M'Barek massive sulphide orebodies, rock types, and selected diamond drill holes (DDH) that are illustrated in Fig. 3and Fig. 7.

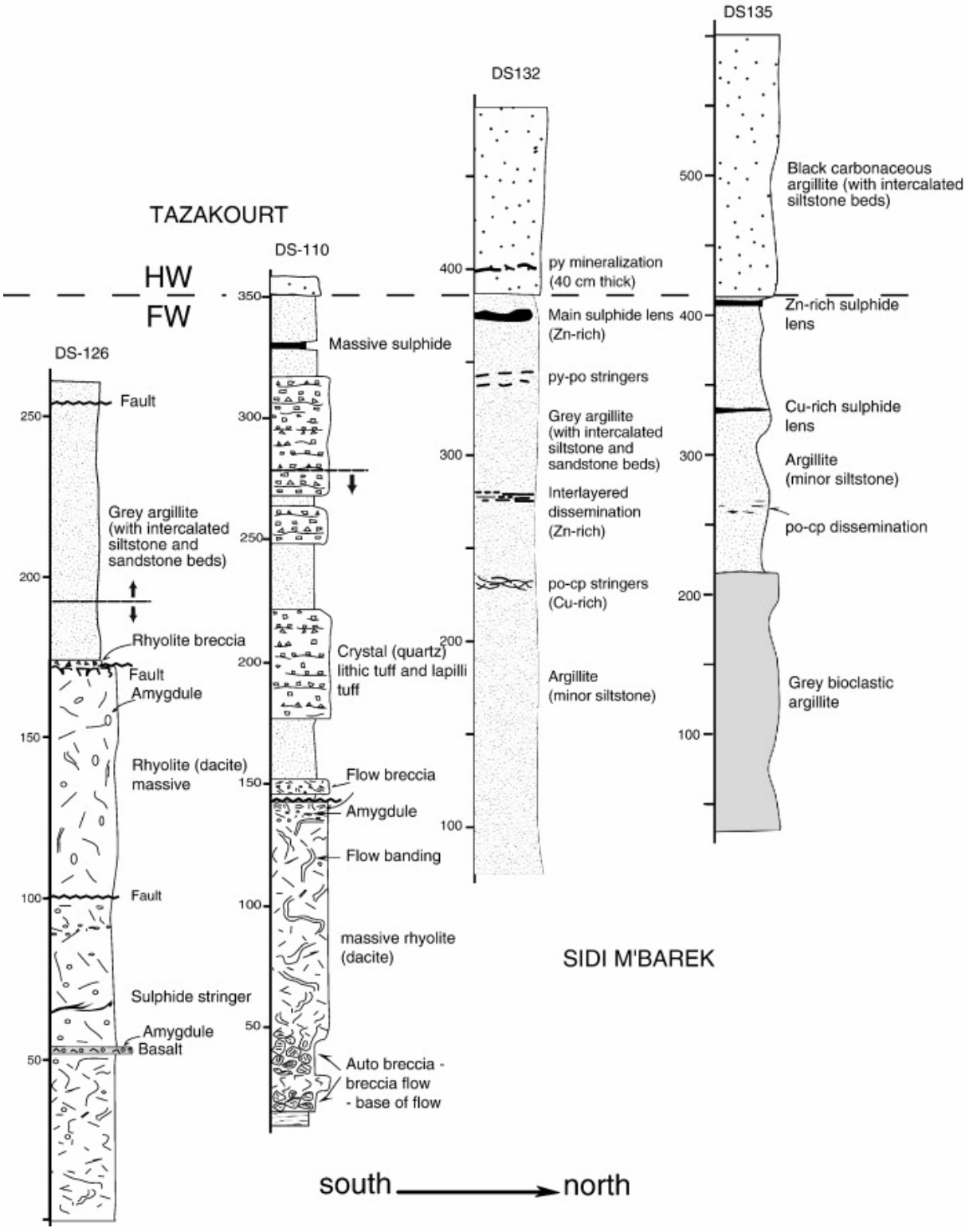

Fig. 3. Restored east–west stratigraphic sections of the Draa Sfar area, drawn from detailed logging of diamond drill holes DS126, DS110, DS125, and DS132. Drill hole locations are shown in Fig. 2.

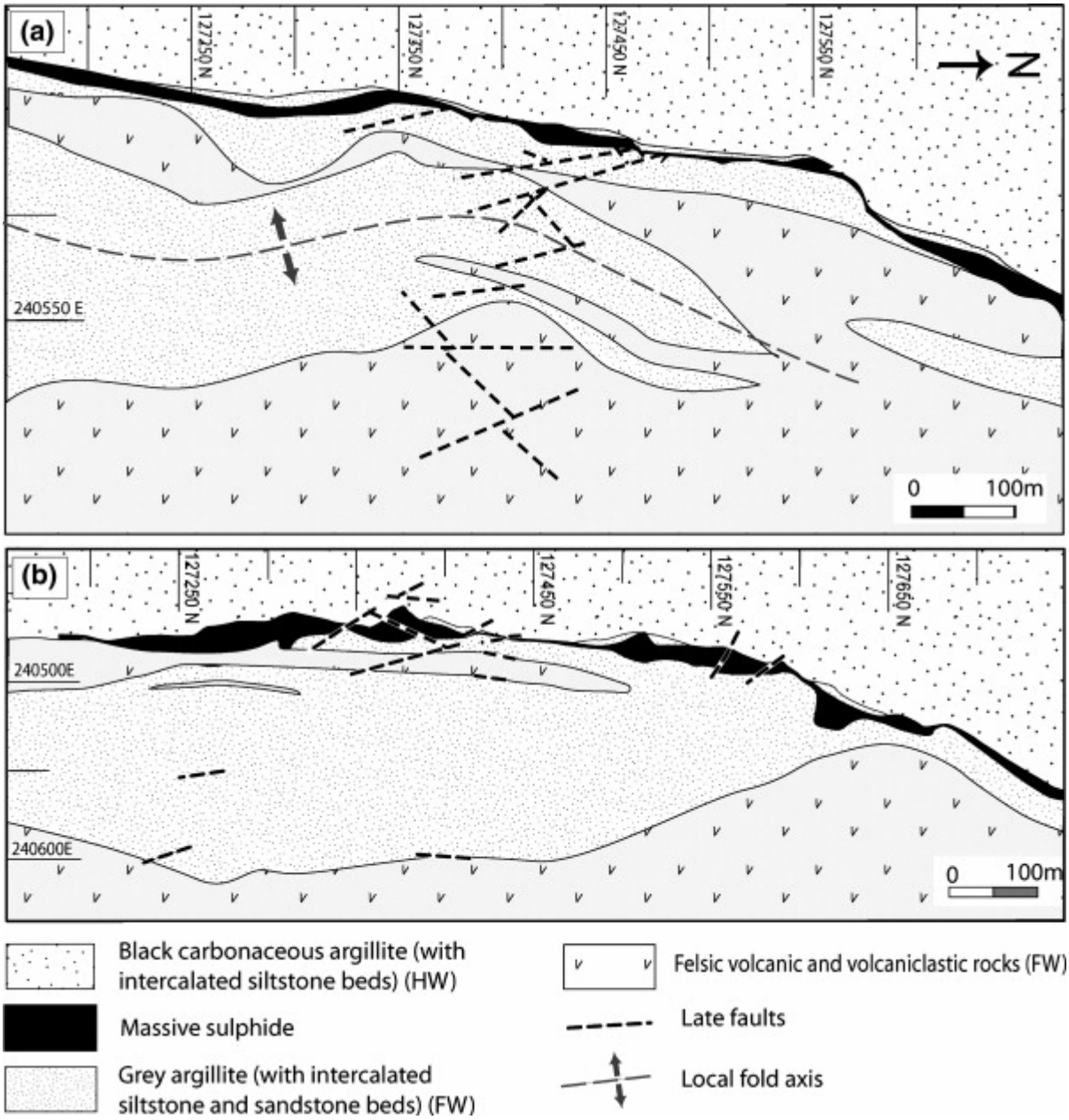

Fig. 4. Simplified geological map of the (a)− 200 and (b)− 300 m levels through the Tazakourt orebody illustrating the sheet-like, pinch and swell form of the sulphide lens.

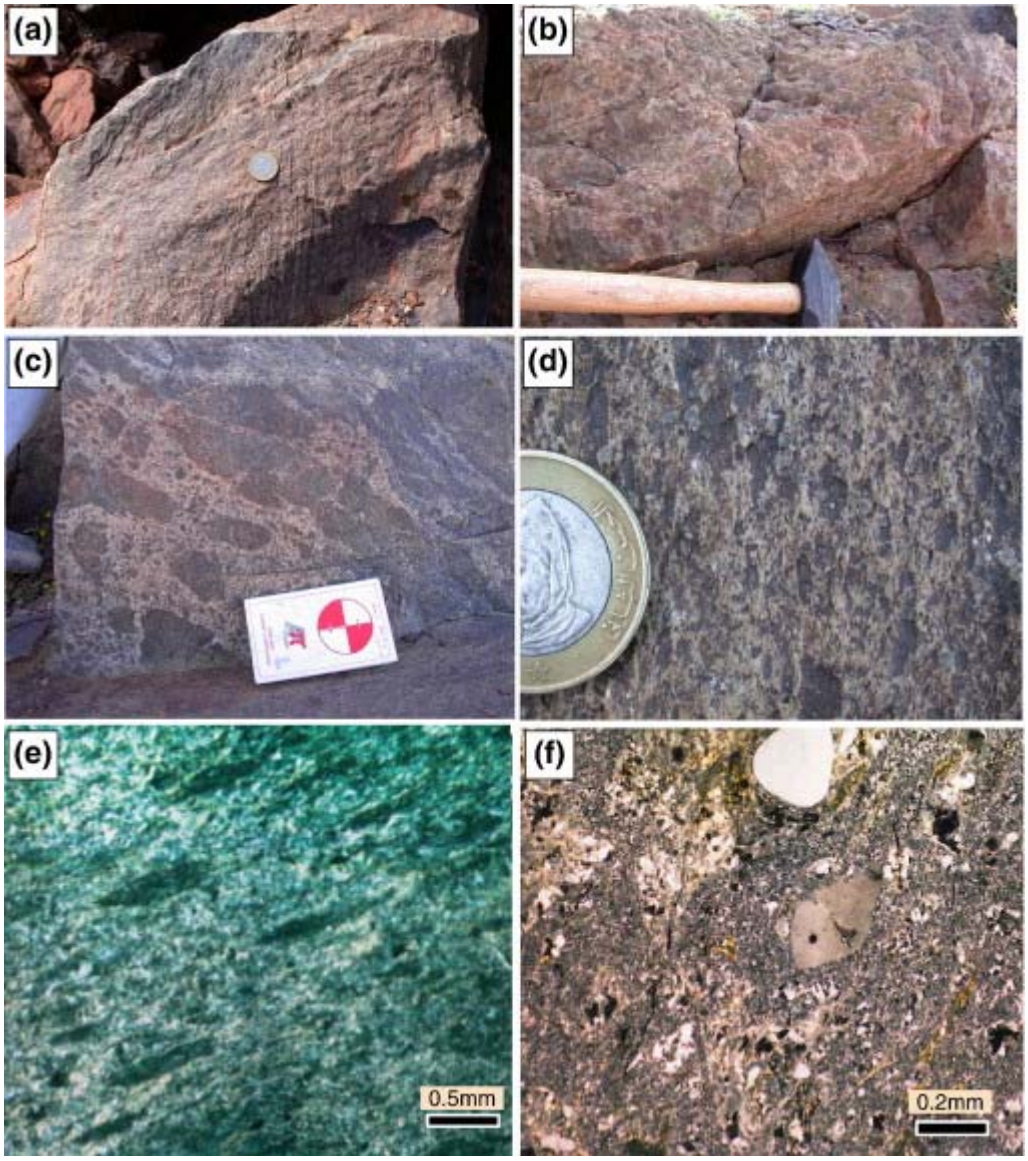

Fig. 5. Representative photographs of least-altered volcanic rocks of the Draa Sfar area: (a) coherent flow-banded rhyodacite, (b) *in situ* brecciated, autoclastic rhyodacitic flow, (c) tuff breccia, (d) quartz crystal, vitric lapilli tuff, (e) foliated vitric lapilli tuff, plane polarized light, and (f) massive rhyodacite showing quartz phenocrysts and spherulites, cross polarized light.

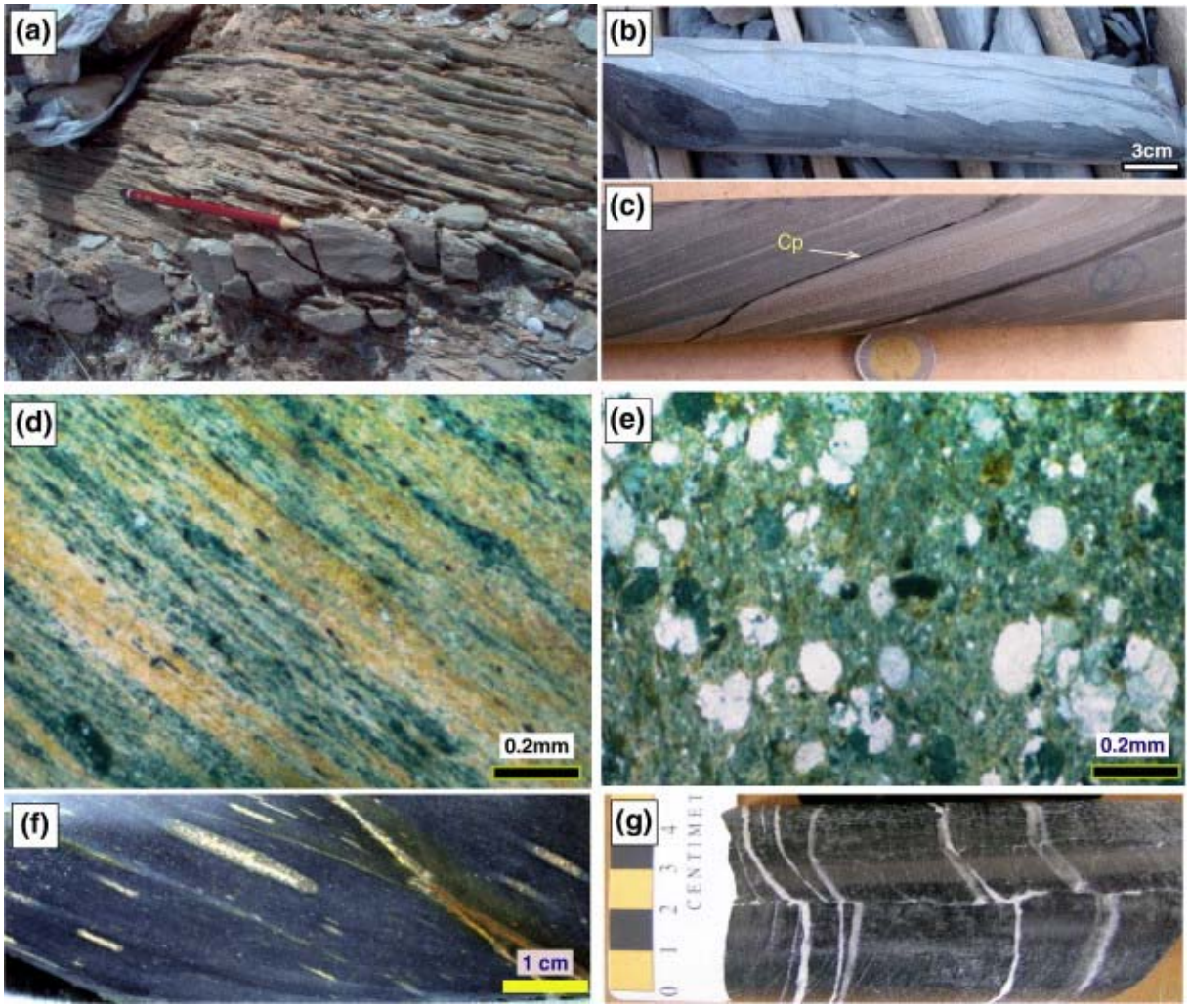

Fig. 6. (a) foliated grey argillite with intercalated siltstone at Tazakourt, (b) black, carbonaceous argillite with thinly laminated siltstone (light) at Tazakourt, (c) disseminated (synsedimentary) chalcopyrite (cp) within siltstone bed intercalated with grey argillite immediately above rhyodacitic volcanic rocks, (d) typical sericite schist at Sidi M'Barek, cross polarized light, (e) quartzitic sandstone, cross polarized light, (f) dark green chloritized argillite (footwall) showing deformed sulphide nodules, and (g) black carbonaceous argillite typical of the hanging wall strata, with calcite layers parallel to S_1.

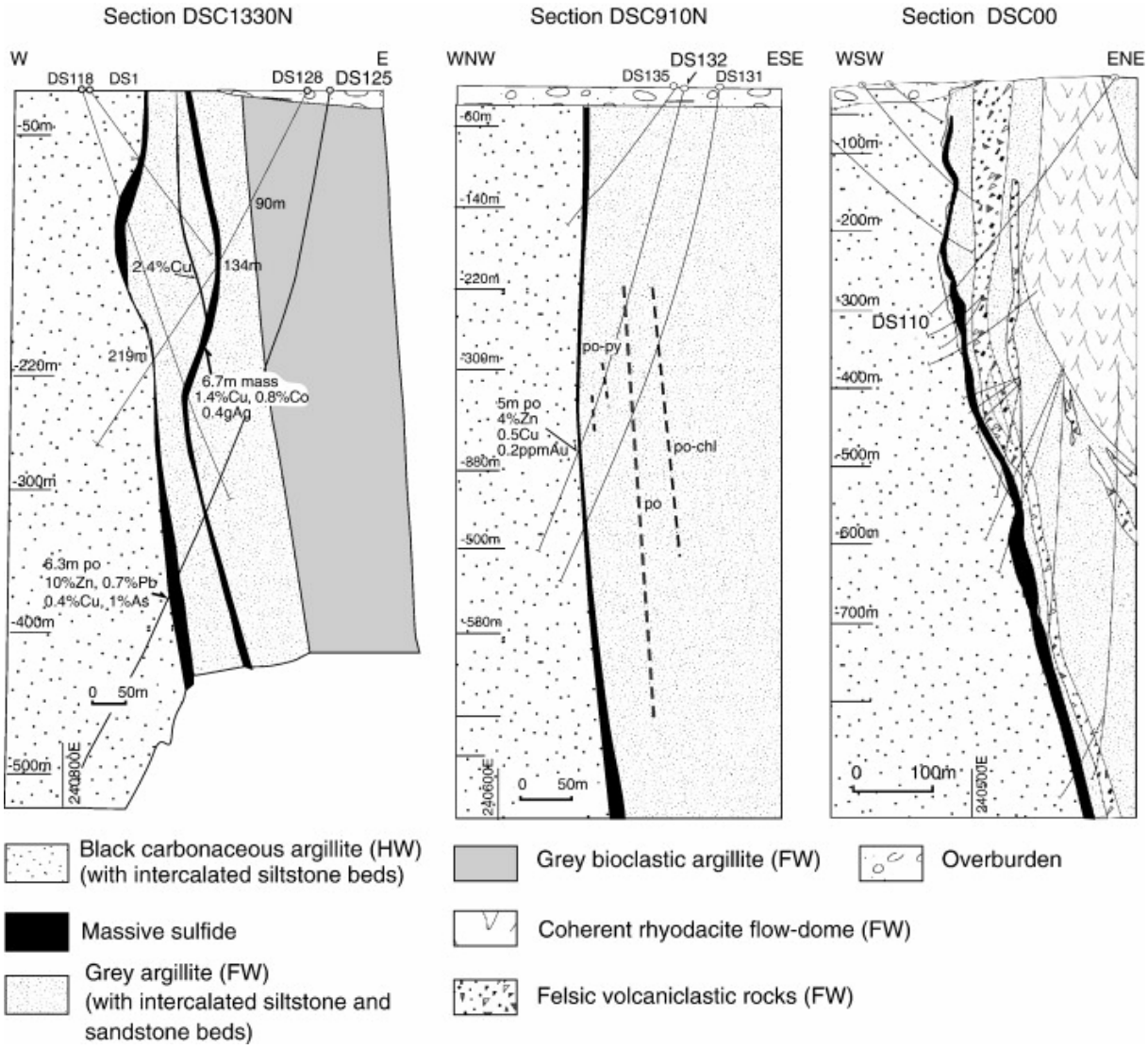

Fig. 7. Vertical east–west cross sections looking north through the Sidi M'Barek (DSC1330N) and Tazakourt (DSC00N and DSC910N) orebodies, showing the massive sulphide lenses and rock types. Note that footwall dykes and sills are not illustrated because of their small scale. Drill hole locations are shown in Fig. 2.

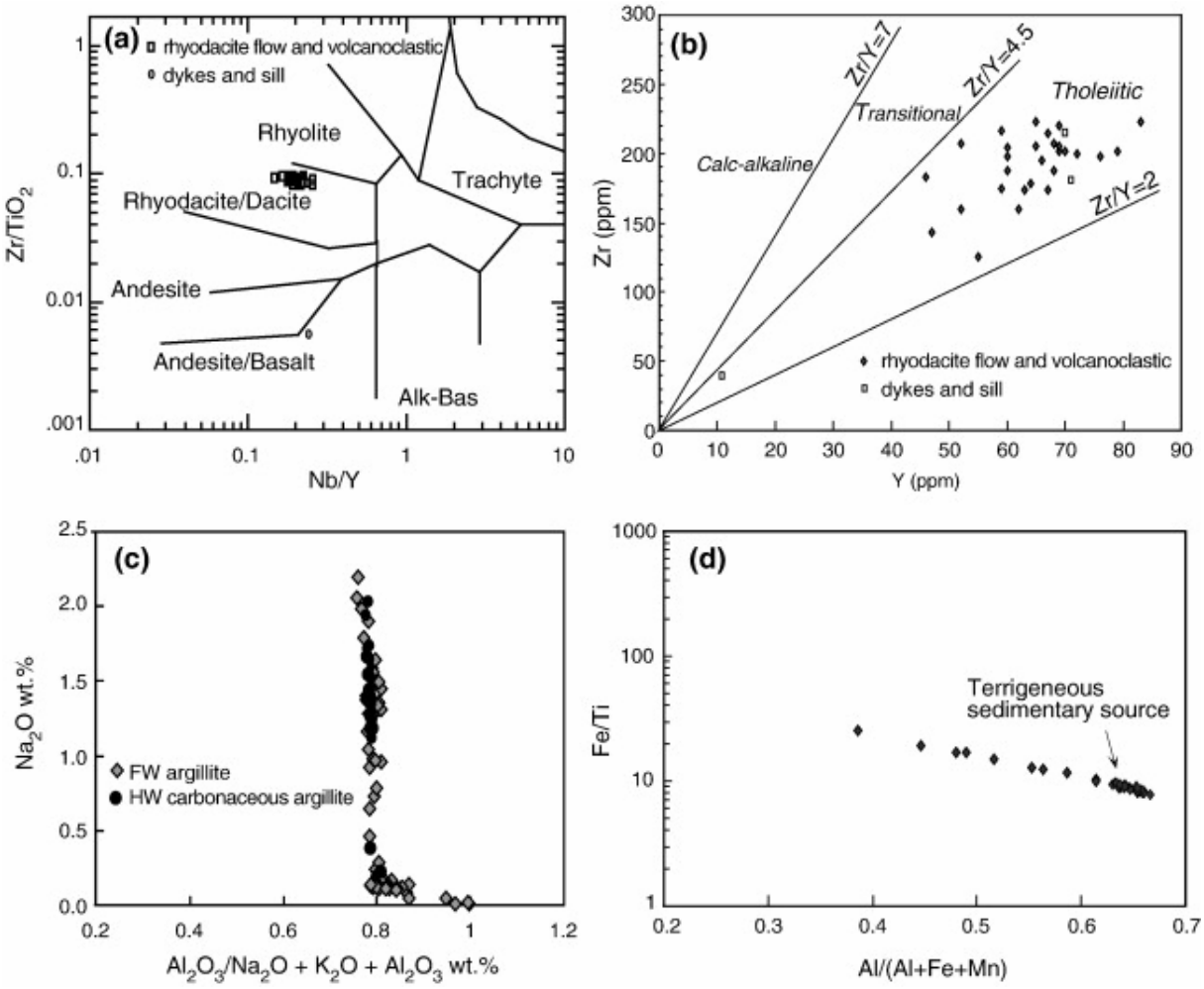

Fig. 8. (a) Winchester and Floyd (1977) Nb/Y *vs.* Zr/TiO_2 classification diagram showing the rhyodacitic composition of felsic volcanic and volcaniclastic rocks (squares), and the basaltic composition of the hanging wall gabbro (circles). (b) Y *vs.* Zr discrimination diagram showing the tholeiitic affinity of rhyodacitic volcanic and volcaniclastic rocks, hanging wall gabbro, and aphanitic footwall mafic dykes (divisions after Barrett and MacLean, 1999). (c) $Al_2O_3 / (Al_2O_3 + Na_2O + K_2O) - Na_2O$ alteration index for the footwall and hanging wall argillite; note that Na_2O values are over 0.65 (Taylor and McLennan, 1985 and Lentz et al., 1995). (d) Plot of Fe/Ti *vs.* Al / (Al + Fe + Mn) for all Draa Sfar argillites ($n = 83$, after Boström, 1973) illustrating the pronounced terrigenous contribution to these rocks.

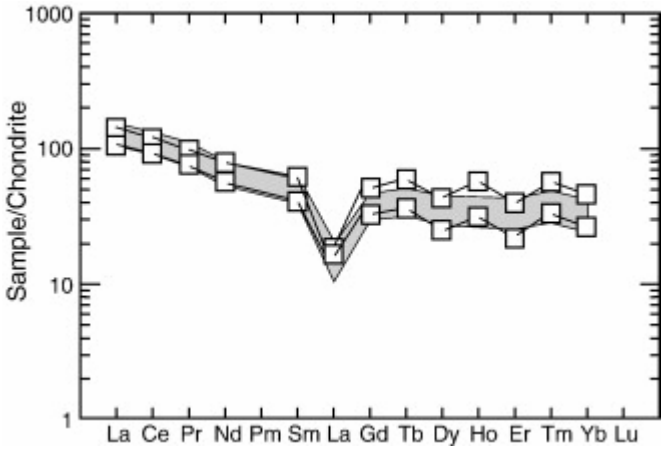

Fig. 9. Chondrite-normalized, rare-earth element profiles for rhyodacitic volcanic and volcaniclastic rocks at Draa Sfar (shaded field) and, for comparison, two least-altered and representative samples of the FIIIb rhyolites that host the Archean, Kidd Creek VMS deposit, Ontario, Canada (squares; Prior et al., 1999). Chondrite-normalization values after Nakamura (1974).

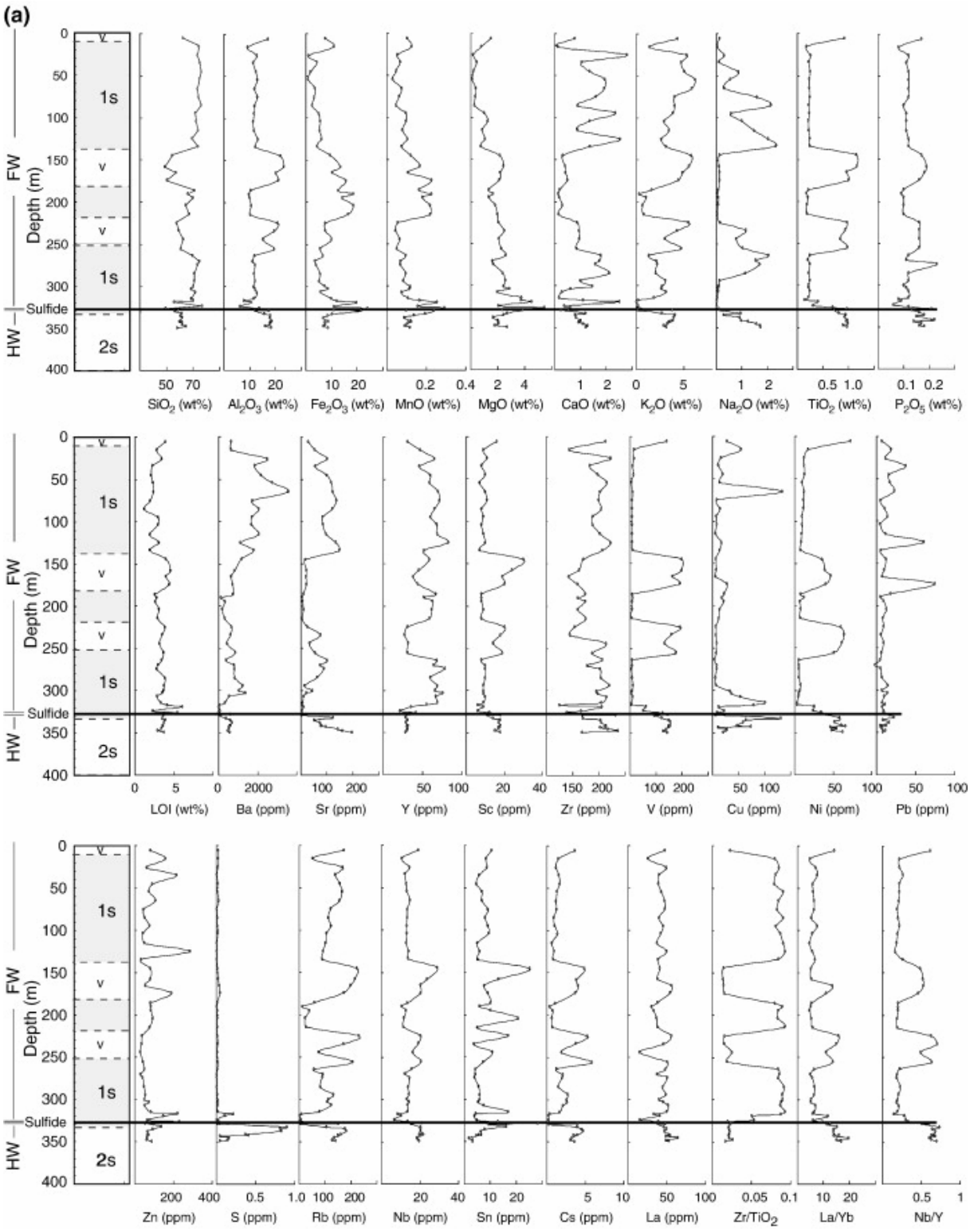

Fig. 10. Geochemical profiles illustrating stratigraphic variations in major and trace elements and immobile-element ratios used to discriminate between rock types for drill holes (a) DS110, (b) DS132, and (c) DS125 (note 1s = argillite, 2s = carbonaceous argillite, V = rhyodacitic volcanic and volcaniclastic rocks).

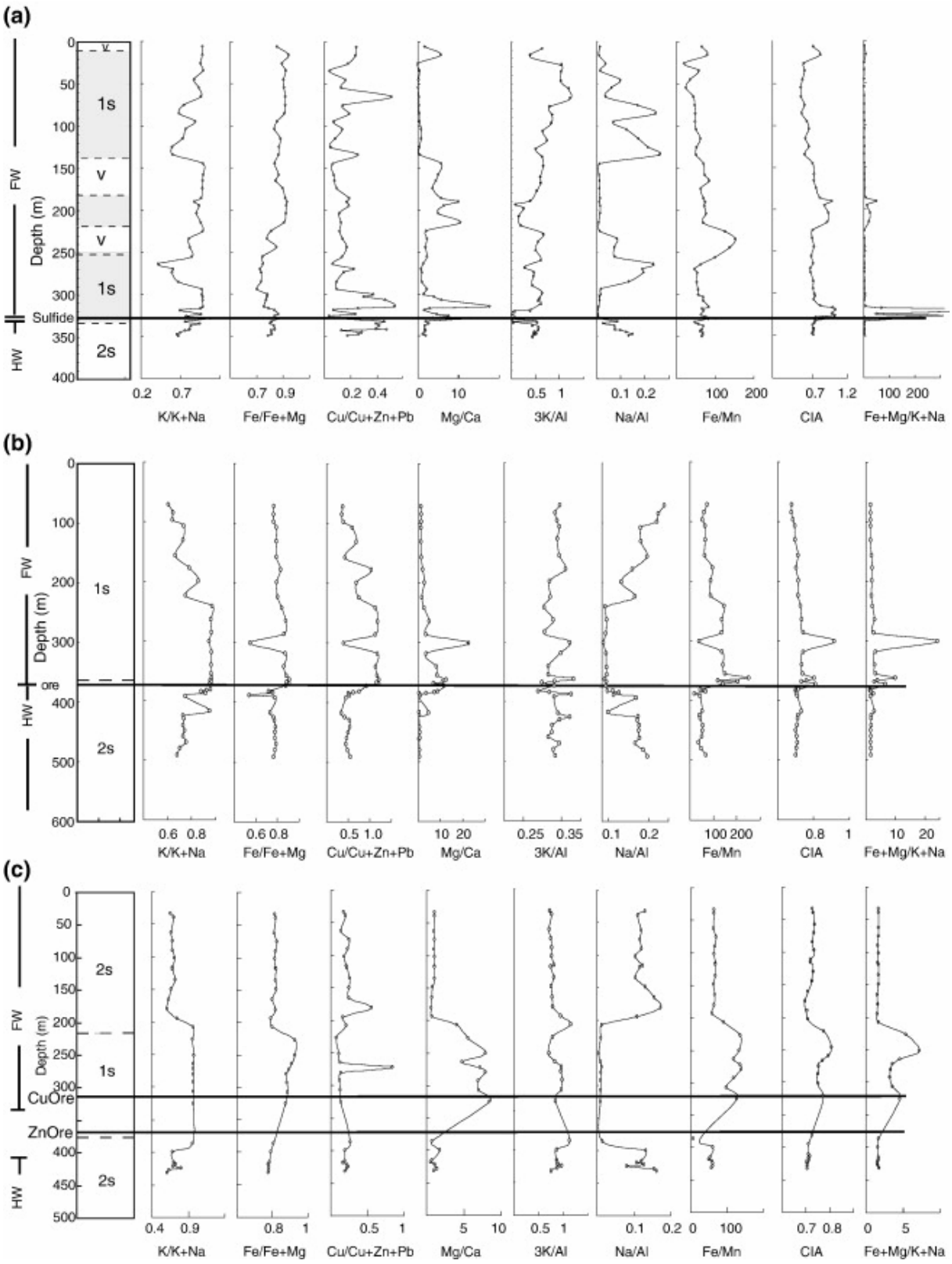

Fig. 11. Stratigraphic and lithologic variations in alteration and paleoenvironment indices for samples from drill holes (a) DS110, (b) DS132, and (c) DS125 (note 1s = argillite, 2s = carbonaceous argillite, and v = rhyodacitic volcanic and volcaniclastic rocks).

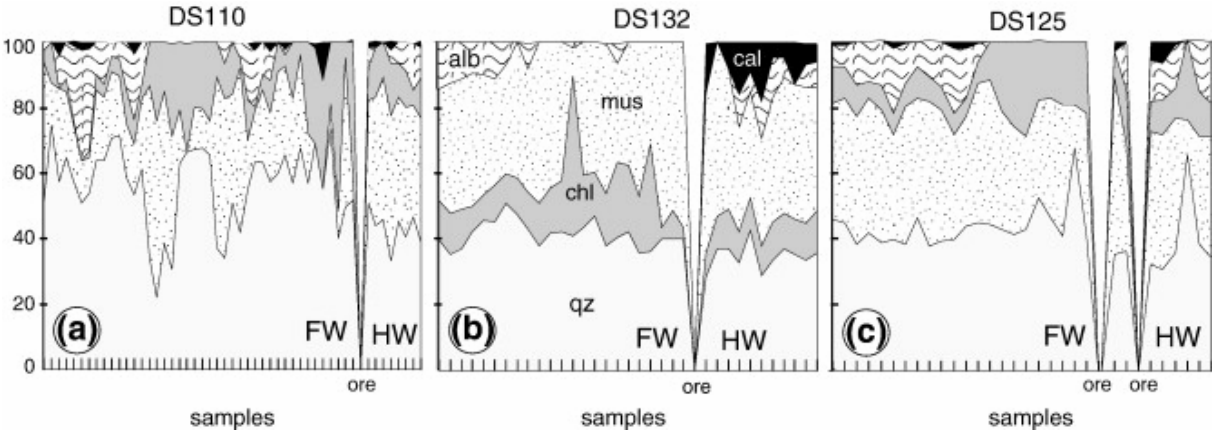

Fig. 12. Variations in the modal percentage of major and minor minerals with distance above and below massive sulphide ore in drill holes DS110 (a), DS132 (b), and DS125 (c) (chl: chlorite, cal: calcite, qz: quartz, ms: muscovite, alb: albite).

Fig. 13. (a) Photomicrograph of (a) footwall tuff showing pervasive chloritization, transmitted plane polarized light, (b) massive chloritized argillite at the contact with massive sulphide at Tazakourt, and (c) syntectonic quartz–chlorite veins located at the top of the Tazakourt massive sulphide lens.

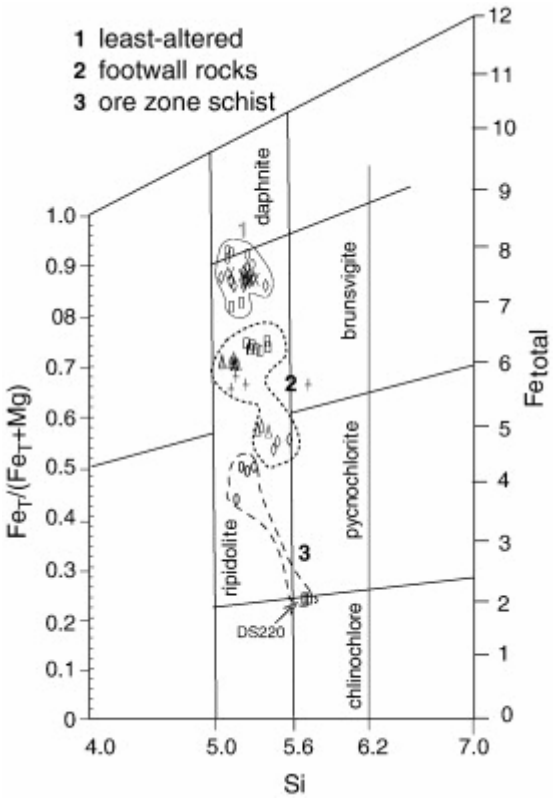

Fig. 14. Chlorite compositions plotted on a Hey (1954) diagram, samples taken from (1) least-altered volcanic rocks and argillite, (2) altered footwall argillite and (3) argillite inclusions within massive sulphide and argillite immediately adjacent to massive sulphide.

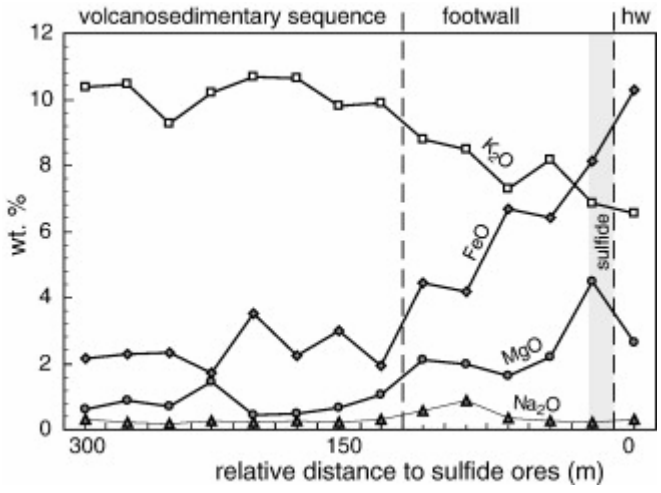

Fig. 15. Variation in the Na_2O, FeO, MgO and K_2O content of sericite within footwall argillite with increasing distance from massive sulphide (from electron microprobe analyses).

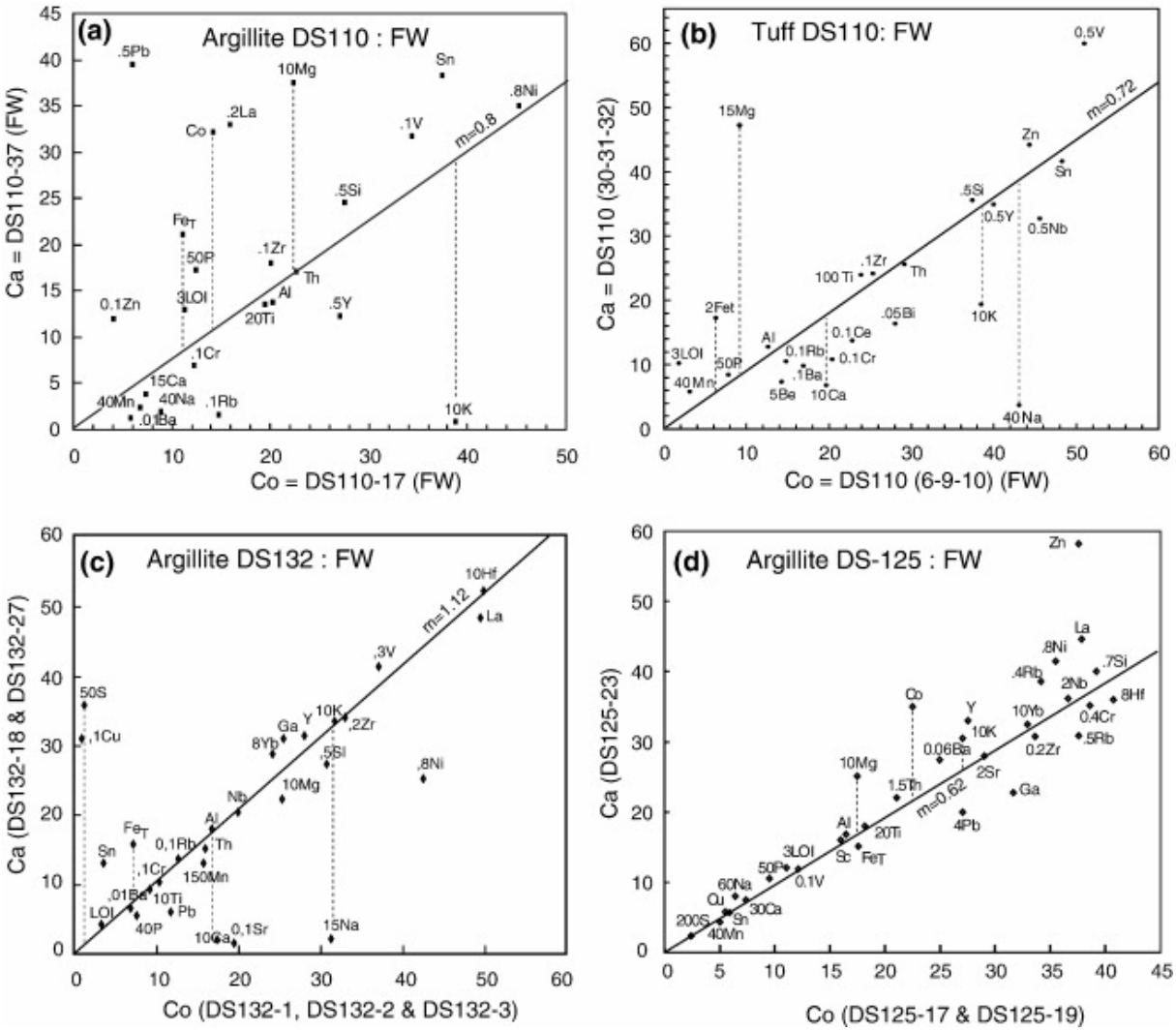

Fig. 16. Isocon diagrams (Grant, 1986) in which least-altered rocks are compared to altered equivalents within the footwall alteration zone. Concentrations are scaled arbitrarily to fit the diagram (*e.g.*, Ca × 2.5; Ba/10). Elements are expressed as oxides and represented on the diagram as symbols; $Fe_{(total)}$ represents total iron. The slope of each isocon is indicated as a value *m* used to calculate mass changes.

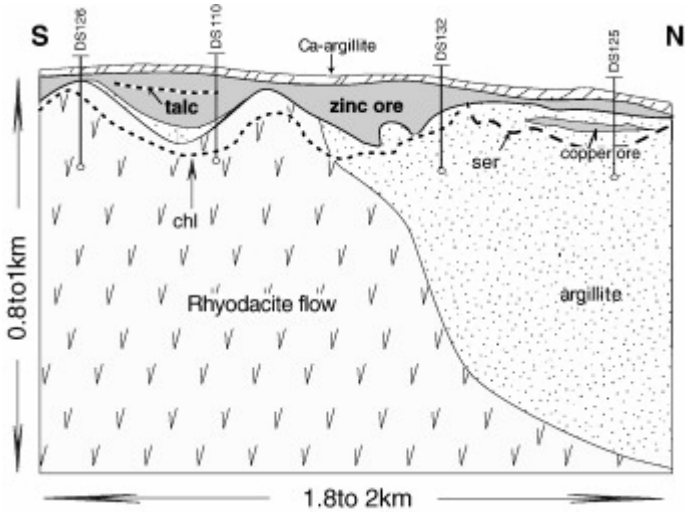

Fig. 17. Schematic reconstruction of the Draa Sfar deposit showing the distribution of rhyodacitic volcanic and volcaniclastic rocks, argillites and the lateral extent of chlorite and sericite alteration associated with the massive sulphide orebodies.

Table 1a. : Representative microprobe analyses of chlorites

	110-33	**DS10**	**110-20**	**110-27**	**110-37**	**131-5**	**132-11**	**132-M2**	**132-M6**	**TDS27**	**TDS24**	**DS220**	**TDS26**
N	**8**	**6**	**8**	**4**	**5**	**3**	**3**	**4**	**4**	**6**	**2**	**2**	**6**
SiO_2	22.81	22.3	22.29	24.58	23.51	25.24	23.57	23.8	24.59	21.75	22.41	28.13	22.32
FeO	33.38	38.89	38.55	27.77	33.36	27.51	33.74	31.46	24.59	39.86	37.09	12.47	38.33
Al_2O_3	22.08	21.13	21.09	21.7	21.43	19.91	21.81	21.39	21.79	20.73	21.64	20.3	21.25
MnO	0.51	0.66	0.51	0.38	0.4	0.42	0.29	0.33	0.95	0.6	0.55	1.63	0.59
MgO	7.77	3.07	3.22	11.54	6.89	12.83	6.53	8.9	14.94	2.12	4.53	22.5	3.21
ZnO	0.02	0.07	0.03	0.04	0.03	0.02	0.13	0	0.17	0.02	0.05	0.03	0.12
Total	86.57	86.12	85.67	86.01	85.6	85.94	86.07	85.87	87.03	85.09	86.27	85.05	85.8
	Structural formulae on the basis of 14 (O,H)												
Si	2.56	2.61	2.61	2.68	2.67	2.76	2.66	2.66	2.62	2.6	2.59	2.86	2.61
Fe	3.14	3.81	3.78	2.53	3.16	2.51	3.19	2.94	2.19	3.98	3.58	1.06	3.75
Mn	0.05	0.07	0.05	0.04	0.04	0.04	0.03	0.03	0.09	0.06	0.05	0.14	0.06
Mg	1.3	0.54	0.56	1.88	1.17	2.09	1.1	1.48	2.37	0.38	0.78	3.41	0.56
Zn	0	0.01	0	0	0	0	0.01	0	0.01	0	0	0	0.01
total	9.98	9.93	9.93	9.92	9.9	9.96	9.89	9.93	10.01	9.94	9.94	9.92	9.92
OH	8	8	8	8	8	8	8	8	8	8	8	8	8
Aliv	1.44	1.39	1.39	1.32	1.33	1.24	1.34	1.34	1.38	1.4	1.41	1.14	1.39
Alvi	1.49	1.52	1.53	1.47	1.53	1.32	1.56	1.48	1.35	1.52	1.53	1.3	1.54
∑ cations	17.98	17.93	17.93	17.92	17.9	17.96	17.89	17.93	18.01	17.94	17.94	17.92	17.92
Fe / Fe + Mg	0.71	0.88	0.87	0.57	0.73	0.55	0.74	0.66	0.48	0.91	0.82	0.24	0.87

Table 1b. : Representative microprobe analyses of white mica

Sample	**132-M2**	**132-M6**	**132-10**	**TDS-24**	**DS10**	**110-2**	**110-20**	**110-27**	**110-35**	**132-4**	**TDS-27**	**132-12**	**TDS 8**	**132-9**
N	**5**	**3**	**5**	**8**	**8**	**4**	**6**	**5**	**3**	**4**	**4**	**5**	**5**	**1**
SiO_2	46.14	41.18	43.12	44.91	46.01	46.08	47.32	46.71	44.57	44.71	45.58	46.21	45.4	44.1
FeO	1.92	8.12	6.42	2.34	2.23	2.14	2.3	1.73	10.27	4.43	3.51	6.66	2.97	4.19
K_2O	9.91	6.86	8.2	9.25	10.62	10.38	10.45	10.19	6.57	8.79	10.67	7.28	9.8	8.49
Na_2O	0.3	0.24	0.26	0.18	0.27	0.31	0.23	0.27	0.3	0.58	0.22	0.34	0.23	0.87
Al_2O_3	32.25	30.56	31.6	32.87	33.69	33.35	32.78	32.83	28.12	28.99	32.19	27.6	32.55	30.45
MgO	1.08	4.48	2.21	0.71	0.5	0.63	0.86	1.44	2.62	2.12	0.45	1.61	0.65	1.96
F	0.4	0.16	0.13	0.18	0.05	0.13	0.32	0.27	0.14	0.19	0.1	0.31	0.32	0
Total	92	91.59	91.93	90.45	93.37	93.03	94.27	93.44	92.58	89.81	92.73	90.02	91.92	90.06

Table 2. :Temperature calculations based on the Al^{iv} chlorite geothermometer[a]

Sample no	**Al^{iv} uncorrected**	**Fe / (Fe + Mg)**	**Al^{iv} corrected**	***T* (°C)**
Group 1 samples see Fig. 13				
TDS24	2.829	0.821	3.404	379
DS10	2.783	0.877	3.397	378
110-20	2.771	0.871	3.38	376
TDS27	2.803	0.913	3.442	383
TDS26	2.776	0.87	3.385	377
Group 2 samples				
110-33	2.874	0.707	3.369	375
110-37	2.667	0.731	3.179	355
131-5	2.486	0.546	2.869	322
132-11	2.68	0.743	3.2	357
132-M2	2.684	0.665	3.149	352
Group 3 samples				
132-M6	2.762	0.48	3.098	346
110-27	2.636	0.575	3.039	340
DS220	2.272	0.237	2.438	276

[a] Following the method of Kranidiotis and MacLean (1987).